A Comprehensive Modeling Study of Hydrogen Oxidation

MARCUS Ó CONAIRE[1], HENRY J. CURRAN[2], JOHN M. SIMMIE[1], WILLIAM J. PITZ[3], CHARLES K. WESTBROOK[3]

[1] *National University of Ireland, Galway, Ireland*
[2] *Galway-Mayo Institute of Technology, Galway, Ireland*
[3] *Lawrence Livermore National Laboratory, Livermore, CA 94551*

Correspondence to: Henry Curran; e-mail:henry.curran@nuigalway.ie

ABSTRACT: A detailed kinetic mechanism has been developed to simulate the combustion of H_2/O_2 mixtures, over a wide range of temperatures, pressures and equivalence ratios. Over the series of experiments numerically investigated, the temperature ranged from 298 to 2,700 K, the pressure from 0.05 to 87 atm, and the equivalence ratios from 0.2 to 6.

Ignition delay times, flame speeds and species composition data provide for a stringent test of the chemical kinetic mechanism, all of which are simulated in the current study with varying success. A sensitivity analysis was carried out to determine which reactions were dominating the H_2/O_2 system at particular conditions of pressure, temperature and fuel/oxygen/diluent ratios. Overall, good agreement was observed between the model and the wide range of experiments simulated.

INTRODUCTION

The prospect of a hydrogen-based economy has prompted increased interest in the use of hydrogen as a fuel given its high chemical energy per unit mass and cleanliness. It appears that most of the technological problems in using hydrogen in spark-ignited internal combustion engines, including NO_x emissions [1], have now been solved; vehicular on-board storage is probably the one remaining difficulty [2, 3].

There is also continued interest in developing a better understanding of the oxidation of hydrocarbon fuels [4] over a wide range of operating conditions in order to increase efficiency and to reduce the emission of pollutant species. All, or almost all petrochemical, fuels are hydrocarbons which burn to form carbon dioxide and water. Thus, the development of a detailed kinetic mechanism for hydrocarbon oxidation necessarily begins with a

hydrogen/oxygen sub-mechanism, followed by the addition of CO chemistry.

In recent years, many kinetic studies of hydrogen oxidation have concentrated on a single set of experimental results obtained either in shock tubes, or in flow reactors or in flames; these have been simulated using a detailed kinetic mechanism. This procedure has been criticised recently by Smith [5] who asserts that uncertainty limits on individual reaction rate constants produce a parameter space of possible mechanisms still too imprecise for accurate prediction of combustion properties such as flame speed or ignition delay, thus requiring additional system data. Smith adds that low pressure and counterflow flames, mixtures in shock tubes, and flow or well-stirred reactors are examples of such experimental environments. It is the aim of this study to apply a hydrogen kinetic mechanism to as broad a range of combustion environments as possible.

There have been a very large number of measurements made on the reaction between hydrogen and oxygen. These include flame speed measurements, burner stabilised flames in which species profiles are recorded, shock tube ignition delay times, and concentration profiles in flow reactor studies. This study aims to simulate these experiments using a detailed chemical kinetic mechanism which takes its origin from Mueller *et al.* [6] in their study of hydrogen oxidation in a flow reactor. Mueller and co-workers validated their mechanism using only their flow reactor data over the temperature range 850–1,040 K, at equivalence ratios of $0.3 \leq \phi \leq 1.0$, pressures of 0.3 to 15.7 atm and residence times of 0.004 to 1.5 s. We have exercised their mechanism against shock-tube data, burner-stabilised flame experiments and flame speed data and have made modifications to some of the kinetic parameters in order to achieve better overall agreement between mechanism simulations and this broader range of experimental results. Previously, Marinov *et al.* [7] had also developed a detailed H_2/O_2 kinetic mechanism to simulate shock tube, flame speed and burner stabilised flame experiments with good agreement between model and experiment but a large body of datasets have become available since then. Therefore, *this study* presents a new detailed chemical kinetic mechanism for hydrogen oxidation but with increased attention paid to experiments conducted at high pressures since internal

combustion engines operate at elevated pressures.

Davis *et al.* [8] have recently presented a re-examination of a H_2/CO combustion mechanism in which they simulated some of the experimental data included in this study. Their work was motivated by new kinetic parameters for the important reaction $\dot{H} + O_2 + M = H\dot{O}_2 + M$ and by new thermodynamic data for $\dot{O}H$, and, had the objective of optimising their H_2/CO model against experiment.

IGNITION DELAYS IN SHOCK WAVES

Schott *et al.* [9] measured ignition delay times of two H_2/O_2/Ar fuel mixtures behind incident shock waves over a wide range of reactant densities in the temperature range 1,085–2,700 K and at 1 atm. Skinner and Ringrose [10] measured the ignition delays of an H_2/O_2/Ar mixture in the temperature range 965–1,076 K and at a reflected shock pressure of 5 atm. Asaba *et al.* [11] performed experiments in the temperature range 1,500–2,700 K, at reflected shock pressures of 178–288 torr, at an equivalence ratio, ϕ, of 0.5 and with 98% argon dilution. Fujimoto *et al.* [12] measured ignition delay times of stoichiometric H_2/O_2/Ar fuel mixtures in the reflected shock pressure range 1.3–5 atm and in the temperature range 700–1,300 K. Hasegawa *et al.* [13] measured ignition delays in the temperature range 920–1,650 K, at a reflected shock pressure of 5.5 atm, with $\phi = 0.25$ at 94% argon dilution. Bhaskaran *et al.* [14] reported ignition delay times for a 29.59% H_2, 14.79% O_2, 55.62% N_2 mixture in the temperature range 1,030–1,330 K and at a constant reflected shock pressure of 2.5 atm.

More recently, Slack [15] studied stoichiometric hydrogen-air mixtures in a shock tube and measured induction times near the second explosion limit. The experiments were performed at a reflected shock pressure of 2 atm in the temperature range 980–1,176 K. Cheng *et al.* [16] reported ignition delay times for a 6.67% H_2, 3.33% O_2, 90% Ar mixture in the temperature range 1,012–1,427 K and at a reflected shock pressure, $P_5 \simeq 1.9$ atm. Koike [17] measured ignition delay times for two hydrogen/oxygen/argon fuel mixtures of incident shock pressure 20 torr in the temperature range 1,000–1,040 K.

In a methane shock-tube study, Hidaka *et al.* [18] carried out some measurements of a $H_2/O_2/Ar$ mixture at 1,250–1,650 K and at reflected shock pressures of 1.6–2.8 bar. Petersen *et al.* [19] measured high pressure (33–87 atm) $H_2/O_2/Ar$ reflected shock ignition delays at 1,189–1,876 K and at an equivalence ratio of 1.0 in every case for six mixtures. Petersen *et al.* [20] measured reflected ignition delay times in three highly dilute $H_2/O_2/Ar$ mixtures at temperatures of 1,010–1,750 K, equivalence ratio range $1.0 \leq \phi \leq 1.47$ and around atmospheric pressure. Finally, Wang *et al.* [21] carried out reflected shock measurements in various H_2/air/steam mixtures at 954–1,332 K and pressures of 3.36–16.63 atm. Hydrogen concentration was 15% of air throughout.

FLAME MEASUREMENTS

Atmospheric Flame Speed Measurements

Very many hydrogen/air flame speed studies have been performed at atmospheric pressure, over various ranges of equivalence ratio. Koroll *et al.* [22] reported data in the equivalence ratio range $0.15 \leq \phi \leq 5.5$, Iijima *et al.* [23] in the range $0.5 \leq \phi \leq 3.9$ and Takahashi *et al.* [24] in the range $1 \leq \phi \leq 4$. However, these data did not account for the effects of flame stretch.

The earliest stretch-corrected atmospheric hydrogen/air flame speed experiments were performed by Wu *et al.* [25] in the range $0.6 \leq \phi \leq 6$. Since then, stretch corrected flame speeds, all of which were performed at 1 atm, have been reported at various equivalence ratio ranges: Egolfopoulos *et al.* [26] ($0.25 \leq \phi \leq 1.5$), Law *et al.* [27] ($0.4 \leq \phi \leq 1.5$), Vagelopoulos *et al.* [28] ($0.3 \leq \phi \leq 0.55$), Dowdy *et al.* [29] ($0.3 \leq \phi \leq 5$), Aung *et al.* [30] ($0.3 \leq \phi \leq 5$) and Tse *et al.* [31] ($0.4 \leq \phi \leq 4$), Fig. 1.

The measurements of Takahashi *et al.* [24] are considerably faster than the rest of the data and 10 % faster than the intermediate values of Tse *et al.* and Dowdy *et al.* at an equivalence ratio of 1.75. The slowest flame speeds are those of Aung *et al.* [30] which have a maximum flame speed of 2.6 m s^{-1} at $\phi = 1.65$. The authors point to possible

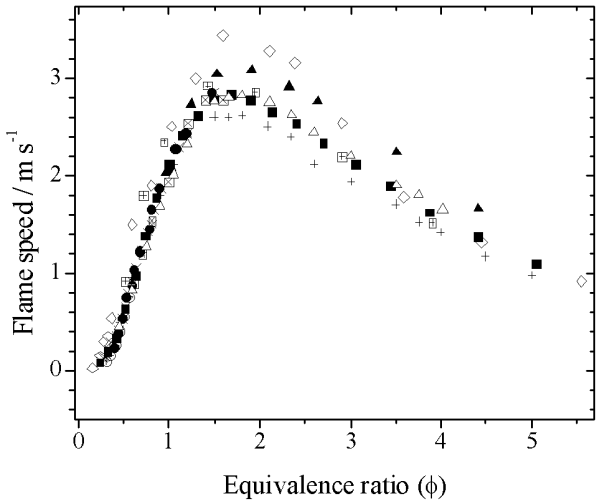

Figure 1: Atmospheric H_2/O_2/air flame speeds *versus* equivalence ratio, $T_i = 298$ K. ◇ Koroll *et al.* [22], ⊞ Iijima *et al.* [23], ▲ Takahashi *et al.* [24]; stretch–corrected: ⊠ Wu *et al.* [25] × Egolfopoulos *et al.* [26], ● Law *et al.* [27], ⊕ Vagelopoulos *et al.* [28], ■ Dowdy *et al.* [29], + Aung *et al.* [30] and △ Tse *et al.* [31].

greater stretch effects than accounted for to explain the relative slowness of their data. The Koroll *et al.* values [22], on the other hand are much faster than any other between $1.0 \leq \phi \leq 2.5$. The recent flame speed measurements of Dowdy *et al.* [29] and Tse *et al.* [31] probably are the most representative of the entire dataset; they have a maximum flame speed of 2.85 m s^{-1} at $\phi = 1.75$.

Lamoureux *et al.* [32] very recently measured the speeds of freely propagating flames in a spherical bomb for five H_2/air mixtures using a diluent consisting of CO_2 + He to mimic the effect of water vapour on flame speed. The mixtures were composed as follows: $x(40\%\mathrm{He} + 60\%\mathrm{CO_2}) + (1 - x)(\mathrm{H_2} + \mathrm{air})$, where x ranged from 0.0 to 0.4, and with *synthetic* air of composition $O_2 : N_2 = 20 : 80$.

High-Pressure Flame Speeds

In addition to their atmospheric flame speed measurements, Tse *et al.* [31] also measured mass burning velocities for H_2/O_2/He mixtures in the equivalence ratio range $0.5 \leq \phi \leq 3.5$

and between 1 and 20 atm at an initial temperature of 298 K. It was reported that flames became increasingly unstable at elevated pressures. For this reason, true stretch-free flame speeds become more difficult to measure. Experimentally, in the case of the 10–20 atm data, the oxygen to fuel ratio was reduced to suppress diffusional-thermal instability and delay hydrodynamic instability. Using helium as the diluent also helped minimize instability up to 20 atm by reducing the Lewis number of the flame and retarding the formation of flame cells. Stretch-free flame speeds have only been available up to a few atmospheres. The oxygen to helium ratio at 1 to 5 atm was 1:7 (12% dilution) and at elevated pressures, this ratio was 1:11.5 (8% dilution).

Burner Stabilised Flame

In their investigation of a rich 18.83 % hydrogen, 4.6 % oxygen, 76.57 % nitrogen flame at atmospheric pressure, Dixon-Lewis *et al.* [33] measured the temperature profile and the concentration profiles of the stable species in the flame, above and below the burner. Flame structure measurements had been carried out by Kohse-Höinghaus [34] who measured $\dot{\mathrm{H}}$ and $\dot{\mathrm{O}}\mathrm{H}$ radical concentrations *versus* distance in a $H_2/O_2/Ar$ flame, at a pressure of 95 mbar, in the equivalence ratio range $0.6 \leq \phi \leq 1.4$ and in the temperature range 1,100–1,350 K. Vandooren and Bian [35] investigated the structure of a rich $H_2/O_2/Ar$ flame over a flat burner at a pressure of 35.5 torr and at an equivalence ratio of 1.91. They reported H_2, O_2, H_2O, $\dot{\mathrm{H}}$, $\dot{\mathrm{O}}$ and $\dot{\mathrm{O}}\mathrm{H}$ species mole fractions *versus* distance above the burner.

Flow Reactors

Mueller *et al.* [6] measured H_2, O_2 and H_2O profiles over the temperature range 850 to 1,040 K, at equivalence ratios of $0.3 \leq \phi \leq 1.0$ in the pressure range from 0.3 to 15.7 atmospheres and over a range of residence times of 0.004 to 1.5 s. Previously, Yetter *et al.* [36] reported atmospheric H_2, O_2 and H_2O profiles at 910 K, and at an equivalence ratio of 0.3.

Experiments Simulated

A representative selection of recent experimental work has been chosen to validate the H_2-O_2 combustion mechanism. The chosen experiments were:

1. the ignition delay times measured by Schott *et al.* [9], Skinner *et al.* [10], Fujimoto [12], Bhaskaran *et al.* [14], Slack [15], Cheng *et al.* [16], Petersen *et al* [19], Hidaka *et al* [18], Petersen *et al.* [20] and Wang *et al.* [21]. Simulations of the data of Asaba *et al.* [11], Hasegawa *et al.* [13], and Koike [17] were not attempted in this study because of a lack of sufficient information.

2. the flame speed measurements of Dowdy *et al.* [29]. These flame speeds not only span a wide range of equivalence ratio but are in agreement with the more recent values of Tse *et al.* [31]. Dowdy and co-workers also measured the temperature profiles, thus making their data more amenable to simulation.

3. the high-pressure flame speed measurements of Tse *et al.* [31]. This data is the only set where hydrogen flame speeds have been measured at pressures greater than 5 atm.

4. the very lean H_2/air and H_2/air/CO_2/He flame speed measurements of Lamoureux *et al.* [32].

5. the burner stabilised flame profiles of Vandooren *et al.* [35] in which reactant and intermediate species concentrations were measured as a function of height above the burner surface. Also included are the species profiles of Dixon-Lewis *et al.* [33].

6. the comprehensive flow reactor data of Mueller *et al.* [6] along with a single data set from Yetter *et al.* [36].

CHEMICAL KINETIC MODELING

The chemical kinetic mechanism was developed and simulations performed using the HCT program [37]. Initially, ignition delay times measured by Slack [15], Fig. 8, and Hidaka *et al.* [18], Fig. 7, and the flow reactor experiments of Mueller *et al.* [6], Fig. 25, were simulated with very good agreement observed between experiment and model. The mechanism was then converted into Chemkin 3.6 [38] format and the simulations repeated in order to compare results from both codes, which were in very good agreement as expected. Thereafter, all other experiments including the flame speeds and the burner stabilised flame profiles were simulated using only the Chemkin applications.

Thermodynamic and Transport Properties

The H_2/O_2 reaction mechanism consists of nineteen reversible elementary reactions, Table 1, together with the thermochemical data, Table 2. Reverse rate constants were computed by microscopic reversibility. The thermochemical data for each species considered in the mechanism are from the Chemkin thermodynamic database [51] with the exception of two:

1. $\Delta H_f(\mathrm{H\dot{O}_2}, 298\mathrm{K})$ of 3.0 kcal mol^{-1}, from Hills and Howard [52] which is in good agreement with the recent reappraisal by Ramond *et al.* [53] of 3.2 ± 0.5 kcal mol^{-1}.

2. $\Delta H_f(\dot{\mathrm{O}}\mathrm{H}, 298\mathrm{K})$ of 8.91 kcal mol^{-1} which is based on recommendations by Ruscic *et al.* [54] and Herbon *et al.* [55].

The Chemkin database of transport parameters was used without modification. As in the study of Tse *et al.* [31], the kinetic parameters of helium were assumed equal to those of argon in order to simulate flame propagation where helium is the diluent. As Tse *et al.* noted, using the third body efficiency of argon for monatomic helium is a useful starting estimate; termolecular reactions such as $\dot{\mathrm{H}} + \mathrm{O_2} + \mathrm{M} = \mathrm{H\dot{O}_2} + \mathrm{M}$ become significant at elevated pressures and so the uncertainties in these values can create considerable differences in the flame speeds.

	Reaction	A	n	E_a	Ref.
	H_2/O_2 Chain Reactions				
1	$\dot{H} + O_2 = \dot{O} + \dot{O}H$	1.91×10^{14}	0.00	16.44	[39]
2	$\dot{O} + H_2 = \dot{H} + \dot{O}H$	5.08×10^{4}	2.67	6.292	[40]
3	$\dot{O}H + H_2 = \dot{H} + H_2O$	2.16×10^{8}	1.51	3.43	[41]
4	$\dot{O} + H_2O = \dot{O}H + \dot{O}H$	2.97×10^{6}	2.02	13.4	[42]
	H_2/O_2 Dissociation/Recombination Reactions				
5[a]	$H_2 + M = \dot{H} + \dot{H} + M$	4.57×10^{19}	-1.40	105.1	[43]
6[b]	$\dot{O} + \dot{O} + M = O_2 + M$	6.17×10^{15}	-0.50	0.00	[43]
7[c]	$\dot{O} + \dot{H} + M = O\dot{H} + M$	4.72×10^{18}	-1.00	0.00	[43]
8[d,e]	$\dot{H} + \dot{O}H + M = H_2O + M$	4.50×10^{22}	-2.00	0.00	[43] $\times 2.0$
	Formation and consumption of $H\dot{O}_2$				
9[f,g]	$\dot{H} + O_2 + M = H\dot{O}_2 + M$	3.48×10^{16}	-0.41	-1.12	[44]
	$\dot{H} + O_2 = H\dot{O}_2$	1.48×10^{12}	0.60	0.00	[45]
10	$H\dot{O}_2 + \dot{H} = H_2 + O_2$	1.66×10^{13}	0.00	0.82	[6]
11	$H\dot{O}_2 + \dot{H} = \dot{O}H + \dot{O}H$	7.08×10^{13}	0.00	0.30	[6]
12	$H\dot{O}_2 + \dot{O} = \dot{O}H + O_2$	3.25×10^{13}	0.00	0.00	[46]
13	$H\dot{O}_2 + \dot{O}H = H_2O + O_2$	2.89×10^{13}	0.00	-0.50	[46]
	Formation and Consumption of H_2O_2				
14[h]	$H\dot{O}_2 + H\dot{O}_2 = H_2O_2 + O_2$	4.2×10^{14}	0.00	11.98	[47]
	$H\dot{O}_2 + H\dot{O}_2 = H_2O_2 + O_2$	1.3×10^{11}	0.00	-1.629	[47]
15[i,f]	$H_2O_2 + M = \dot{O}H + O\dot{H} + M$	1.27×10^{17}	0.00	45.5	[48]
	$H_2O_2 = \dot{O}H + O\dot{H}$	2.95×10^{14}	0.00	48.4	[49]
16	$H_2O_2 + \dot{H} = H_2O + \dot{O}H$	2.41×10^{13}	0.00	3.97	[43]
17	$H_2O_2 + \dot{H} = H_2 + H\dot{O}_2$	6.03×10^{13}	0.00	7.95	[43] $\times 1.25$
18	$H_2O_2 + \dot{O} = \dot{O}H + H\dot{O}_2$	9.55×10^{06}	2.00	3.97	[43]
19[h]	$H_2O_2 + \dot{O}H = H_2O + H\dot{O}_2$	1.0×10^{12}	0.00	0.00	[50]
	$H_2O_2 + \dot{O}H = H_2O + H\dot{O}_2$	5.8×10^{14}	0.00	9.56	[50]

a	Efficiency factors are: H_2O=12.0; H_2=2.5;
b	Efficiency factors are: H_2O=12; H_2=2.5; Ar = 0.83; He = 0.83;
c	Efficiency factors are: H_2O=12; H_2=2.5; Ar = 0.75; He = 0.75;
d	Original pre-exponential A factor is multiplied by two here.
e	Efficiency factors are: H_2O=12; H_2=0.73; Ar = 0.38; He = 0.38;
f	Troe parameters; reaction 9: $a = 0.5$, $T^{\star\star\star} = 1.0\times^{-30}$, $T^{\star} = 1.0 \times 10^{+30}$, $T^{\star\star} = 1.0 \times 10^{+100}$ reaction 15: $a = 0.5$, $T^{\star\star\star} = 1.0\times^{-30}$, $T^{\star} = 1.0 \times 10^{+30}$.
g	Efficiency factors are: H_2=1.3; H_2O=14; Ar = 0.67; He = 0.67;
h	Reactions 14 and 19 are expressed as the sum of the two rate expressions.
i	Efficiency factors are: H_2O=12; H_2=2.5; Ar = 0.45; He = 0.45;

Table 1: Revised H_2/O_2 reaction mechanism. Units: cm^3, mol, s, kcal, K.

Species	ΔH_f^{298K}	S^{300K}	Specific heat capacity, C_p					
			300 K	400 K	500 K	800 K	1000 K	1500 K
$\dot{H}$	52.098	27.422	4.968	4.968	4.968	4.968	4.968	4.968
$\dot{O}$	59.56	38.500	5.232	5.139	5.080	5.016	4.999	4.982
$\dot{O}H$	8.91	43.933	6.947	6.992	7.036	7.199	7.341	7.827
H_2	0.00	31.256	6.902	6.960	6.997	7.070	7.209	7.733
O_2	0.00	49.050	7.010	7.220	7.437	8.068	8.350	8.721
H_2O	−57.77	45.154	8.000	8.231	8.446	9.223	9.875	11.258
$H\dot{O}_2$	3.00	54.809	8.349	8.886	9.465	10.772	11.380	12.484
H_2O_2	−32.53	55.724	10.416	11.446	12.346	14.294	15.213	16.851
N_2	0.00	45.900	6.820	7.110	7.520	7.770	8.280	8.620
Ar	0.00	37.000	4.900	4.900	4.900	4.900	4.900	4.900
He	0.00	30.120	4.970	4.970	4.970	4.970	4.970	4.970

Table 2: ΔH_f(298.15 K) kcal mol^{-1}, S(300 K) and C_p(T) in cal mol^{-1} K^{-1}

Mechanism Formulation

The kinetic mechanism referred to in this study as '*this study*' or the '*revised mechanism*' has its origins in the $CO/H_2/O_2$ reaction mechanism of Yetter *et al.* [56], which was updated later by Kim [57] and is, for the most part, taken from the more recent work of Mueller *et al.* [6].

We found it necessary to modify some of the kinetic parameters of Mueller *et al.* in order to achieve an overall improvement with all the experimental data simulated here. This altered version of the mechanism, Table 1, the *revised mechanism*, reproduces the selected experimental datasets more accurately than that published by Mueller and co-workers.

The entire data set has also been simulated using relevant portions from Leeds 1.5 [58], Konnov [59, 60] and GRI-Mech 3.0 [61] which are all primarily methane oxidation mechanisms. The reason for using both Konnov mechanisms is that the shock tube data presented in Figs. 4-6 was used to validate version 0.3 while the more recent version 0.5 was used to simulate the remaining data. A select set of experiments is reproduced here using GRI-Mech, Leeds and Konnov as an indication of their performance but they have not been comprehensively tested.

Mechanism	Listed reactions	Duplicate reactions	Actual reactions
this study	21	4	19
Mueller *et al.*	29	4	27
GRI-Mech 3.0	30	6	27
Leeds 1.5	23	2	22
Konnov 0.3	24	2	23
Konnov 0.5	29	4	27

Table 3: A comparison of the mechanisms tested.

A comparison shows that these mechanisms are quite different, Table 3; not only do the total number of reactions differ but so do the rate constant expressions.

Reaction Kinetics

It will be clarified later why we made the modifications we did but for now let us look at those that have been made. One of the rate expressions that we modified was:

$$\dot{H} + \dot{O}H + M = H_2O + M$$

Fig. 2 illustrates a selection of experimental and review kinetic recommendations for this reaction from Tsang and Hampson [43], Gay *et al.* [62], Baulch *et al.* [63], Troe [64], Zellner *et al.* [65] and Bulewicz *et al.* [66]. Between 1,250 and 2,000 K, there is at least a one hundred-fold range in reported experimental and review data. The revised rate constant, see Table 1, is twice the recommendation of Tsang and Hampson.

Most of the data for the reaction: $H_2O_2 + \dot{H} = H_2 + H\dot{O}_2$ lies between 700 and 1,100 K. The data plotted alongside our revised rate constant for this reaction, Fig. 3, include the experimental data of Baldwin and Jackson [67] in addition to the review data of Baulch *et al.* [63], Tsang *et al.* [43], Lee *et al.* [68], Baldwin and Walker [69], and Gorse *et al.* [70].

In a recent study, Michael *et al.* [71] measured the rate constant of the reaction $\dot{H} + O_2 + M = H\dot{O}_2 + M$. The measured rate constants for the collision partners nitrogen and argon are in good agreement with our estimates and so it was decided to adhere to the estimated rate constants and efficiencies.

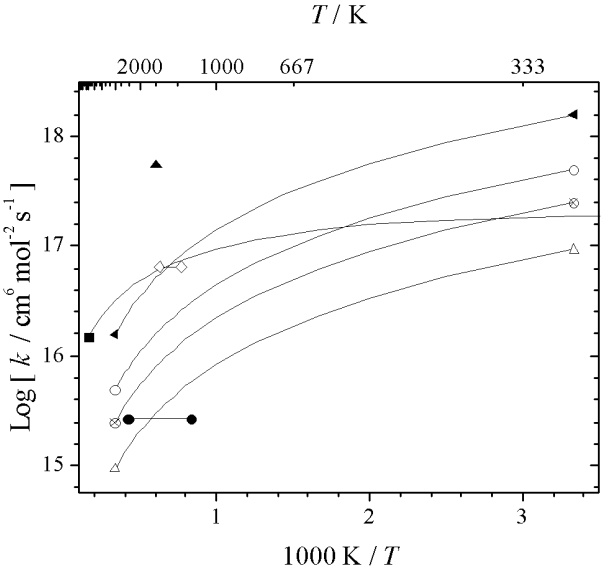

Figure 2: $\dot{H} + \dot{O}H + M = H_2O + M$. ○ *this study*, ⊗ Tsang *et al.* [43] (used by Mueller and co-workers), ● Gay *et al.* [62], △ Baulch *et al.* [63], ■ Troe *et al.* [64], ◇ Zellner *et al.* [65], ▲ Bulewicz *et al.* [66], ◀ Baulch *et al.* [63].

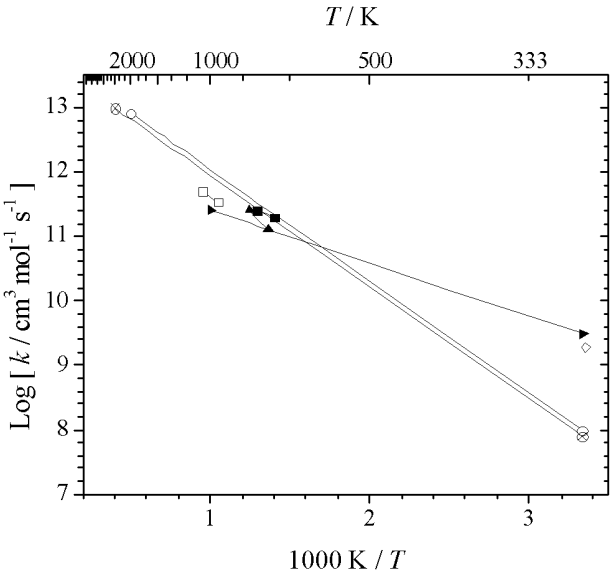

Figure 3: $H_2O_2 + \dot{H} = H\dot{O}_2 + H_2$. ○ *this study*, ⊗ Tsang *et al.* [43] (used by Mueller and co-workers), ▶ Baulch *et al.* [63], ■ Baldwin and Jackson [67], □ Lee *et al.* [68], ▲ Baldwin and Walker [69] and ◇ Gorse *et al.* [70].

Simulating Experimental Conditions

Senkin [72] or Aurora [73] compute the time evolution of a homogeneous reacting gas mixture in a closed system. This includes predicting the chemical behaviour behind incident and reflected shock waves in a shock tube and species evolution in a laminar flow reactor. A limiting case, frequently applied when simulating reactions in shock waves and also used in this study, assumes a constant volume (density) boundary which we used to simulate reflected shock ignition delay times. The Shock code [74] was used to simulate ignition delay times behind incident shocks.

We used the application Premix [75] to model time-independent, adiabatic freely propagating (expanding spherical) flame speeds in addition to species and intermediate concentration profiles in a burner stabilised flame. In order to allow for changes in the structure of the flame with time, a re-gridding strategy is included which involves the computation of the optimum grid as part of the time-dependent solution. We used the standard Chemkin transport package, with thermal diffusion included and increased the number of grid-points until the flame speed converged. Mixture averaged transport properties were employed. Some modeling workgroups such as Resources Research Institute, University of Leeds prefer to use the multi-component transport option. Lawrence Livermore National Laboratories use the mixture averaged transport properties as we do.

Shock Tube

Konnov [59,60] used the experiments of Schott and Kinsey along with those of Skinner and Ringrose, to validate version 0.3 of his mechanism at temperatures of 965–2,700 K. In both studies, ignition delays below 1,200 K correspond to the time of maximum [$\dot{\mathrm{O}}\mathrm{H}$]; above 1,200 K they correspond to the time at which [$\dot{\mathrm{O}}\mathrm{H}$] = 10^{-6} mol dm^{-3}. In addition, both studies plotted the experimental data as the concentration of molecular oxygen multiplied by the ignition delay time *versus* temperature. Figs. 4–6 depict both sets of experimental results with Konnov's mechanism predictions in addition to those of our current mechanism

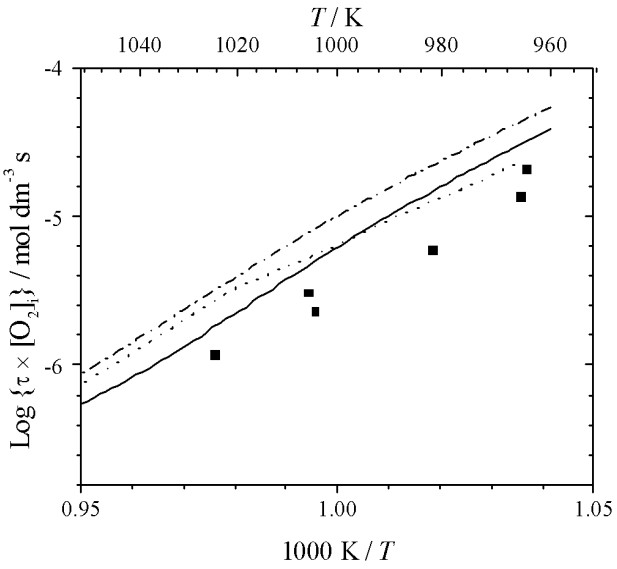

Figure 4: $\tau \times [O_2]$ vs. $1/T$ ■ Skinner and Ringrose [10] 8% H_2 + 2% O_2 + balance Ar, at 1 atm. —— *this study*, - - - - Mueller *et al.*, $\cdots$ Konnov 0.1–0.3, [59].

and those of Mueller *et al.* Both our predictions and those of Mueller *et al.* are identical except for Skinner *et al.* and are in overall good agreement with the experimental data.

The ignition delay times, τ, measured by Hidaka and co-workers correspond to the tangent to the maximum rate of increase in water concentration, $(d[H_2O]/dt)_{\max} = \tau$, and were thus calculated in our simulations with very good agreement between our model (the Mueller mechanism gives identical results) and experiment, Fig. 7.

Slack [15] measured ignition delay times in stoichiometric hydrogen/air mixtures at a reflected shock pressure of two atmospheres. The revised mechanism performed very well over the entire temperature range in simulating the experimental data, Fig. 8. The Mueller *et al.* mechanism on the other hand, predicts slower ignition times, particularly at temperatures below 1,025 K.

The mechanism is in good agreement with the ignition delays of Fujimoto [12], particularly between 900 and 1,100 K, Fig. 9, although the mechanism is too slow at temperatures below 950 K.

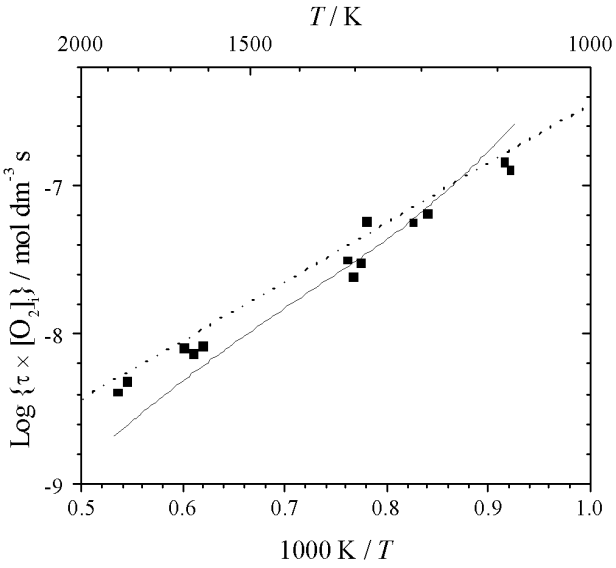

Figure 5: $\tau \times [O_2]$ vs. $1/T$ ■ Schott and Kinsey [9] 1% H_2 + 2% O_2 + balance Ar, at 1 atm. —— *this study* and Mueller *et al.*, ··· Konnov 0.1–0.3, [59].

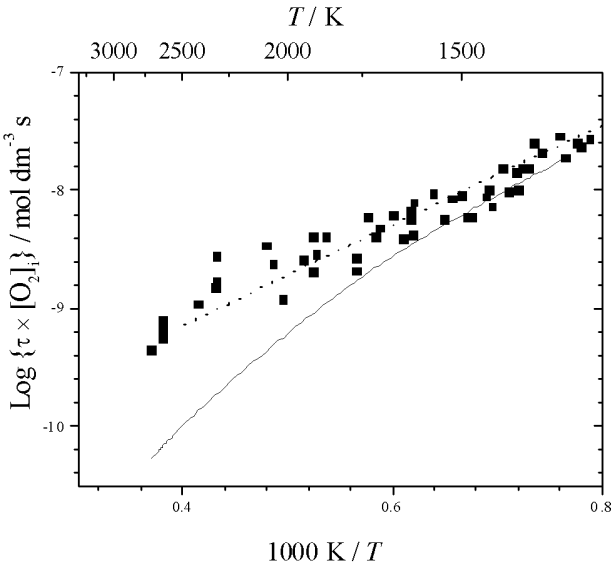

Figure 6: $\tau \times [O_2]$ vs. $1/T$ ■ Schott and Kinsey [9] 4% H_2 + 2% O_2 + balance Ar, at 1 atm. —— *this study* and Mueller *et al.*, ··· Konnov 0.1–0.3, [59].

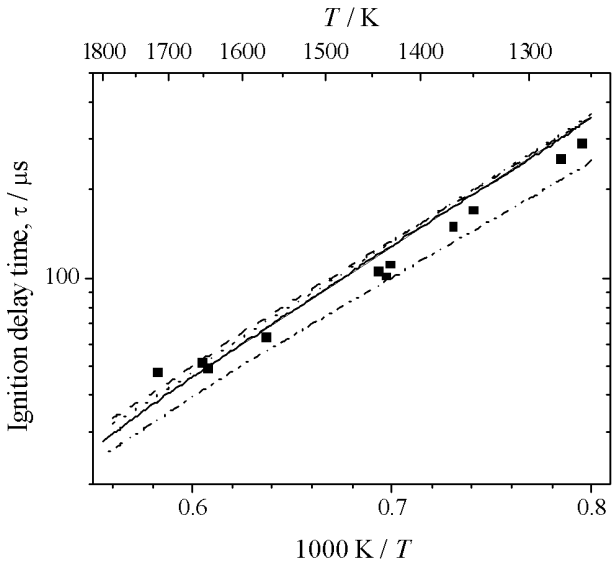

Figure 7: Ignition delay measurements 1.0% H_2 + 1.0% O_2, balance Ar, at 3 bar; Hidaka *et al.* [18] ■; model predictions —— *this study* and Mueller *et al.*, – – – Leeds 1.5, ··· GRI-Mech 3.0, – · – Konnov 0.5.

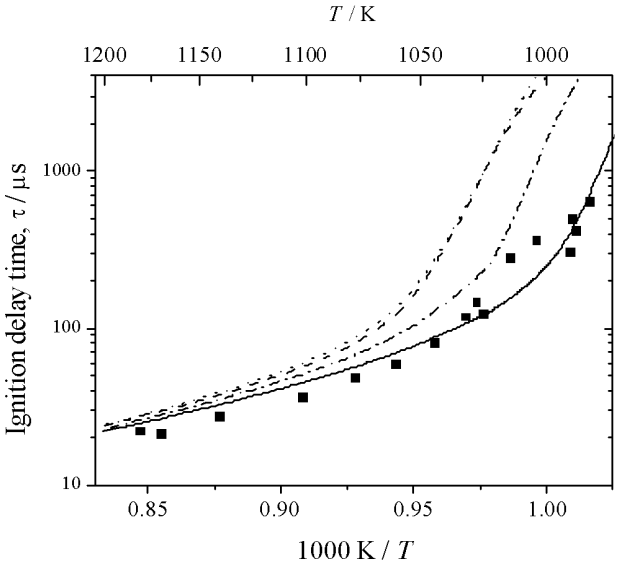

Figure 8: Ignition delay times of stoichiometric H_2/air, at 2 atm, from Slack [15]: ■; model predictions —— *this study*, – – – – Mueller *et al.* and Mueller *et al.* with ϵ (H_2)=1.3 for $\dot{H} + O_2 + M = H\dot{O}_2 + M$, – – – Leeds 1.5, ··· GRI-Mech 3.0 and Konnov 0.5.

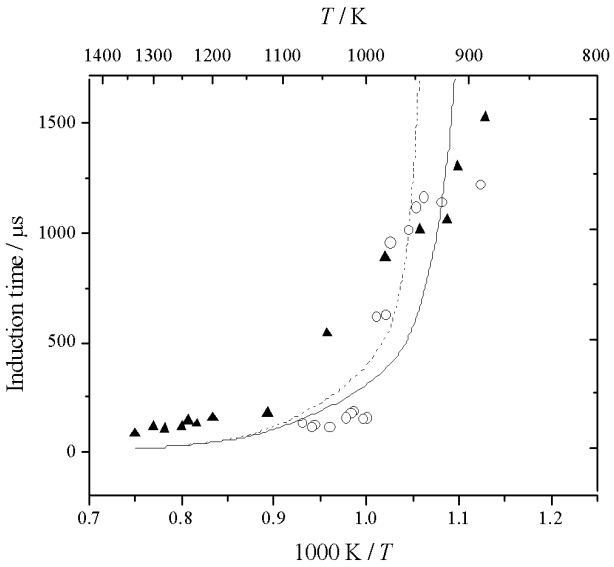

Figure 9: Ignition delay times for stoichiometric H_2/air, from Fujimoto *et al.* [12]: ▲ light emission, ○ pressure; —— *this study*, – – – Mueller *et al.*

The results of Petersen *et al.* [19] along with model predictions are shown in Fig. 11. Three sets of data from the same study, in the pressure range 33–64 atm and in the temperature range 1650–1930 K have also been simulated with good agreement, but are not shown here. The ignition delays were measured as the tangent of the pressure profile *versus* time. Fig. 13 illustrates the difference between the ignition delay time measured from the onset of temperature rise and the ignition time measured by the tangent of the pressure profile. The more recent atmospheric shock tube measurements of Petersen *et al.* [20], Figs. 12 and 13, are also reproduced with reasonable success by our mechanism although the experiments shown in Fig. 12 are considerably faster than those predicted by *this study* and Mueller *et al.* For this set of data, the ignition delay time could not be determined from the simulated pressure or temperature profiles at high temperatures, simply because the pressure and temperature did not give an unambiguous ignition delay time as the mixtures were very dilute; so, the ignition delay time was re-defined, in this case only, as the time corresponding to a maximum in the product of the concentrations of $\dot{O}H$

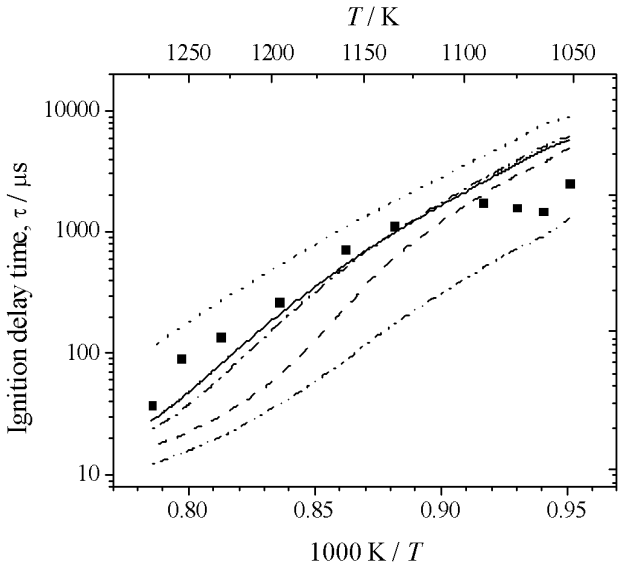

Figure 10: Ignition delay times for a hydrogen/air mixture at 0.3–0.5 MPa [21] *versus* model predictions: —— *this study*, - - - - Mueller *et al.*, - - - Leeds 0.5, $\cdots$ GRI-Mech 3.0, — - - Konnov 0.5. Mixture composition: 11.25% H_2, 63.75% air, 25% steam.

and $\dot{O}$, that is $[\dot{O}] \times [\dot{O}H]$. Two additional sets of data from that study, in the temperature range 1,100–1,520 K and at 1 atm were simulated with good agreement but are not shown here. The measurements of Cheng *et al.* and Bhaskaran *et al.* are replicated well in *this study*; rotational relaxation of N_2 was not taken into consideration. Given that atomic species substantially decrease the vibrational relaxation rate [76, 77], this is probably a reasonable assumption for Fig. 8 and 15.

The experiments of Wang *et al.* [21] are well reproduced although only one datset is shown here, Fig. 10. The only significant discrepancies arise for the 0% and 15% steam mixtures, where the measured ignition delay times are a lot faster than those predicted by the models below 1,010 and 1,090 K respectively.

The improved predictions are a result of choosing a third-body efficiency of 1.3 for H_2 in the reaction $\dot{H} + O_2 + M = H\dot{O}_2 + M$, whereas Mueller *et al.* adopted a value of 2.5. This has resulted in the improvements seen in the simulation of the ignition delays of

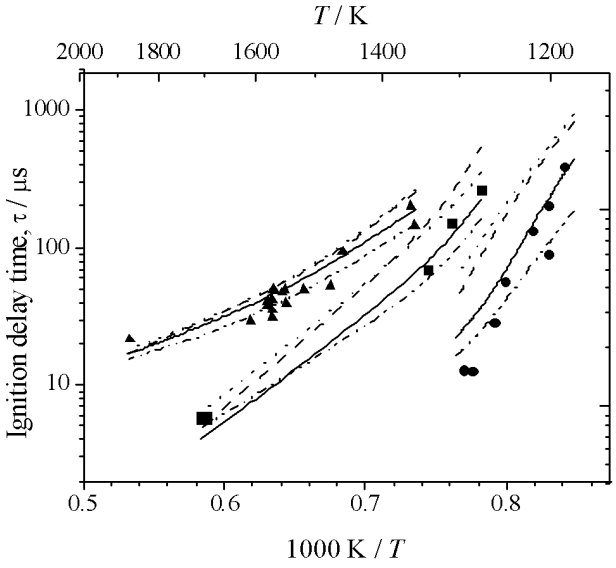

Figure 11: Ignition delay times for stoichiometric $H_2/O_2/Ar$ [19]; ■ 0.5% H_2 + 0.25% O_2, 64–87 atm; ● 2.0% H_2 + 1.0% O_2, 33 atm; ▲ 0.1% H_2 + 0.05% O_2, 64 atm; model predictions: —— *this study* and Mueller *et al.*, – · –, – – – Leeds 0.5, · · · GRI-Mech 3.0, – · · – Konnov 0.5.

Slack, Fig. 8, and those of Fujimoto *et al.*, Fig. 9.

Freely Propagating Flames

As far back as 1972, Andrews and Bradley [78] demonstrated that laminar flame speeds could be substantially modified by aerodynamic stretch. Aerodynamic flame strain (or stretch) is caused by preferential mass and thermal diffusion along with flow divergence. Depending on the influence of experimental conditions the flame can undergo positive or negative stretch which must be adjusted to give a flamespeed that contains a minimal amount of stretch. The influence of stretch is more pronounced in hydrogen flames than in other fuels due to its highly diffusive nature. Only in the last ten years has there been a concerted effort to minimize these effects. Uncertainty in the scatter of flame speed data needs to be minimized in order to assess the effectiveness of proposed kinetic schemes for flame propagation.

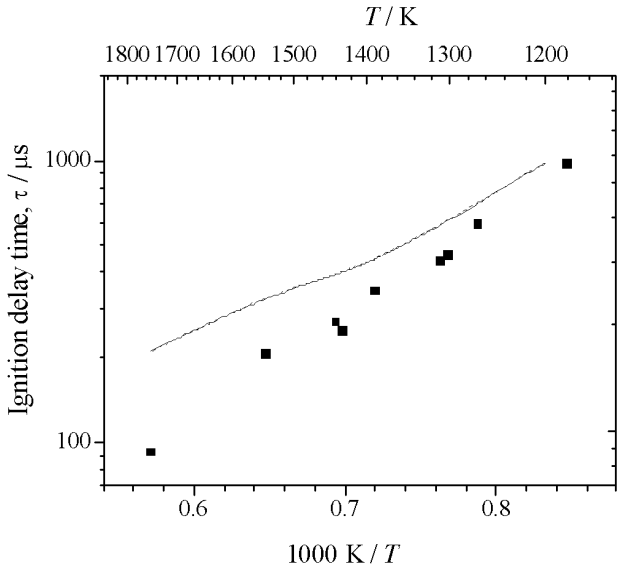

Figure 12: Ignition delay measurements [20]: ■ 1.03% H_2 + 0.5% O_2, balance Ar, at $\simeq 1$ atm; model predictions —— *this study* and Mueller *et al.*

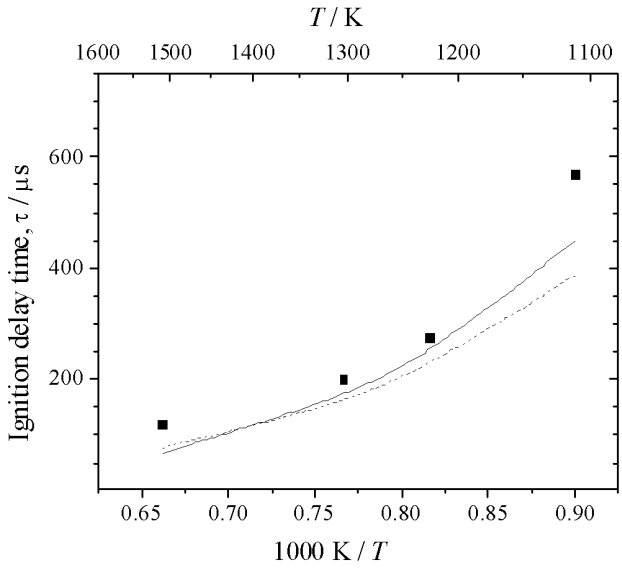

Figure 13: Ignition delay times [20]: ■ 1.03% $H_2 + 0.5\%$ O_2, balance Ar, at $\simeq$ 1 atm; model predictions —— based on pressure-rise, - - - based on temperature-rise.

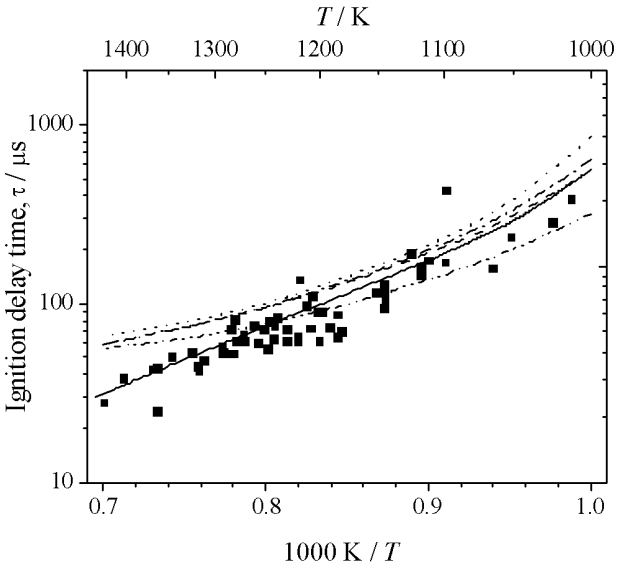

Figure 14: Ignition delay times from Cheng and Oppenheim [16]: ■ 6.67% H_2 + 3.33% O_2, balance Ar, at $\simeq$ 1.9 atm; model predictions —— *this study*, - - - - Mueller *et al.*, - - - Leeds 0.5, · · · GRI-Mech 3.0, — - - Konnov 0.5.

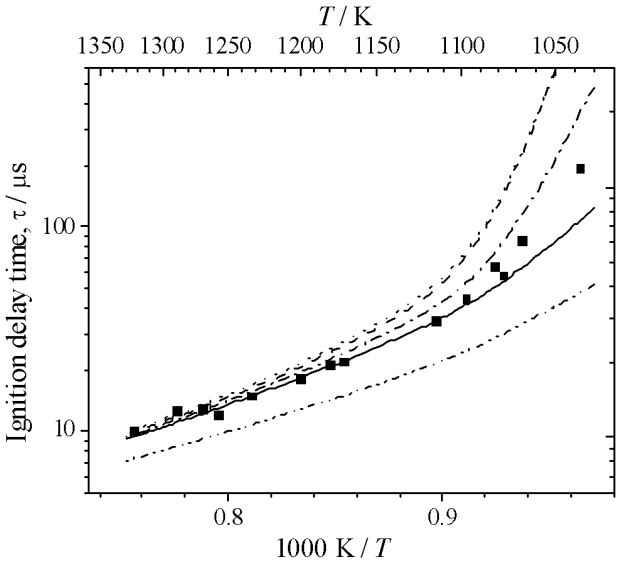

Figure 15: Ignition delay measurements from Bhaskaran *et al.* [14]: ■ 22.59% H_2 + 14.79% O_2, balance N_2, at 2.5 atm; model predictions —— *this study*, - - - - Mueller *et al.*, - - - Leeds 0.5, · · · GRI-Mech 3.0, — - - Konnov 0.5.

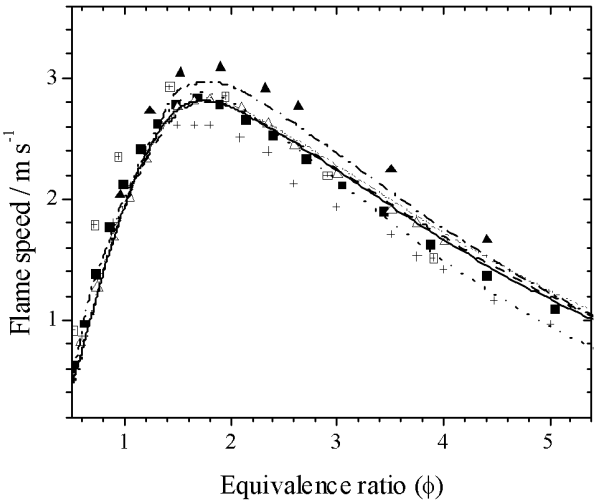

Figure 16: H_2/O_2/air flame speeds *versus* equivalence ratio; 1 atm, 298 K. ▲ Takahashi *et al.* [24], △ Tse *et al.* [31], ■ Dowdy *et al.* [29], + Aung *et al.* [30], ⊞ Iijima *et al.* [23]; —— *this study*, - - - - Mueller *et al.*, – – – Leeds 0.5, · · · GRI-Mech 3.0, — · · Konnov 0.5.

Hydrogen/Air Freely Propagating Flame

Freely propagating premixed hydrogen/air flame speeds at atmospheric pressure were simulated as a function of fuel/oxygen equivalence ratio and the model predictions compared to the selected set of experiments, Fig 16.

The original mechanism lies between Tse *et al.* [31] and the uncorrected results of Takahashi *et al.* [24] but does not adequately represent the stretch-free measurements of Dowdy *et al.* [29] and Tse *et al.*; the revised mechanism is in excellent agreement with these experiments, Fig. 16. An increase by a factor two in the recommended rate constant of the reaction $\dot{H} + \dot{O}H + M = H_2O + M$ resulted in a closer fit to the experimental data represented in the NIST database [79] and lowered simulated atmospheric flame speeds from stoichiometric to rich conditions by up to 7% at maximum burning velocity.

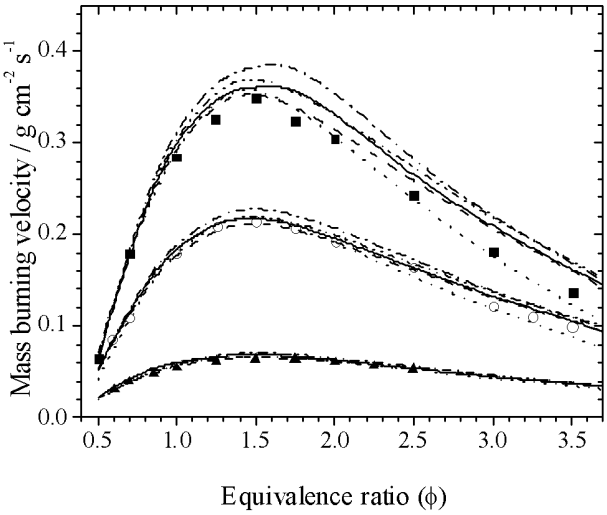

Figure 17: Mass burning velocities for H_2/O_2/He flames,O_2 : He = 1 : 7; Tse *et al.* [31] ■ 1 atm, ○ 3 atm, ▲ 5 atm. model predictions —— *this study*, - - - - Mueller *et al.*, - - - Leeds 0.5, · · · GRI-Mech 3.0, ▬ · · Konnov 0.5.

Hydrogen/Oxygen/Helium Freely Propagating Flame

The measured H_2/O_2/He mass burning rates of Tse *et al.* [31] spanned the pressure range 1 to 20 atm. Mueller *at al.* tends to over-estimate the mass burning velocity, Fig. 17. As the pressures increase, so there is an increasing overestimation of the predicted burning velocity calculated using the Mueller mechanism, with our current mechanism in very good agreement with the experimental data, Fig. 18.

Fig. 20 depicts the mass burning velocity as a function of pressure for the two distinct He : O_2 mixtures; the revised mechanism fits the data substantially better than the mechanism of Mueller *et al.* particularly for the high dilution mixture.

Lean Hydrogen/Air with and without CO_2/He diluent

The experiments of Lamoureux *et al.* were simulated with only limited success. Of the five mixtures, H_2/air/CO_2/He, for which there are results it was not possible to simulate mixtures $x = 0.3$ and 0.4 and the remainder could not be simulated across the complete

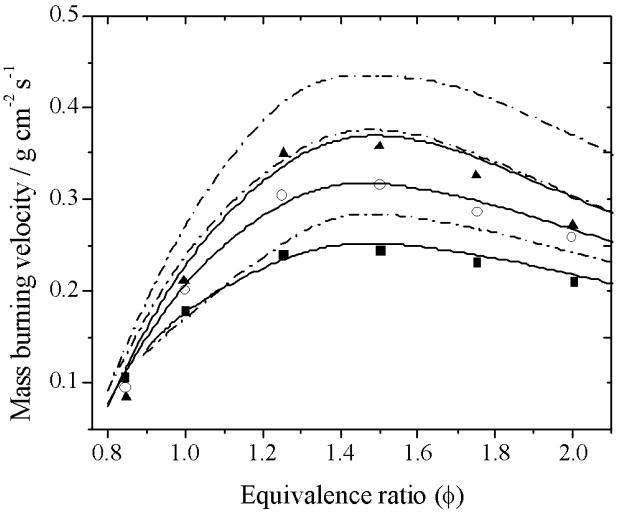

Figure 18: Mass burning velocities for H_2/O_2/He flames, O_2 : He = 1 : 11.5; Tse *et al.* [31] ■ 10 atm, ○ 15 atm, ▲ 20 atm. model predictions ——— *this study*, – – – Mueller *et al.*

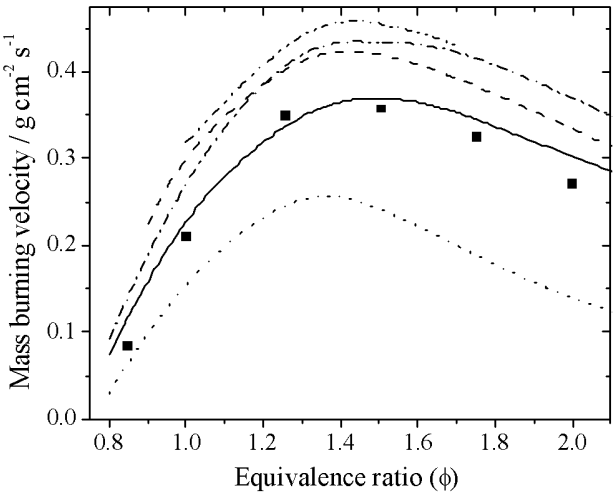

Figure 19: Mass burning velocities for H_2/O_2/He flames, O_2 : He = 1 : 11.5; Tse *et al.* [31] at 20 atm. model predictions ——— *this study*, – – – – Mueller *et al.*, – – – Leeds 0.5, ··· GRI-Mech 3.0, — · — Konnov 0.5.

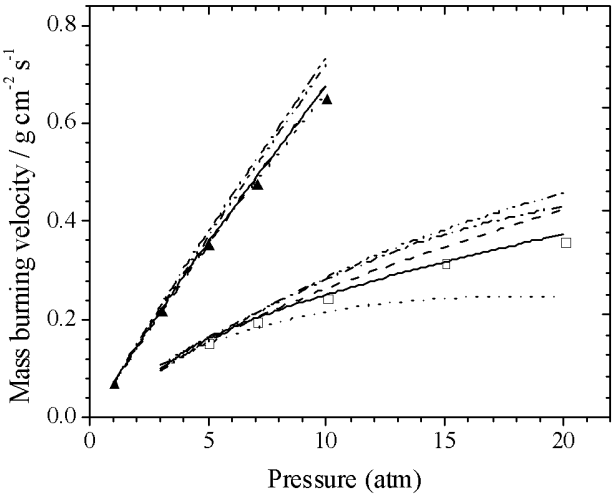

Figure 20: Mass burning velocities for H_2/O_2/He flames *versus* pressure at $\phi = 1.5$; Tse *et al.* [31] ▲ O_2 : He = 1 : 7, □ O_2 : He = 1 : 11.5. model predictions ——— *this study*, - - - - Mueller *et al.*, – – – Leeds 0.5, · · · GRI-Mech 3.0, — · — Konnov 0.5.

range of measured equivalence ratio. This was because the Premix code is less likely to converge with increasingly lean H_2/air mixtures and more so with added carbon dioxide and helium. The simulated flame speeds are consistently slower than the measured values in the equivalence ratio range $0.5 \leq \phi \leq 0.7$. It is pertinent to note that the measurements we did simulate successfully were all up to 20% faster than simulations.

The major factors affecting a change in the flame speed, particularly at elevated pressures are:

1. An increase by a factor two in the recommended rate constant of the reaction $\dot{H} + \dot{O}H + M = H_2O + M$ lowered simulated flame speeds especially at higher pressures from stoichiometric to rich conditions by up to 16% at maximum burning velocity. The 1, 3, 5, 10, 15 and 20 atm burning velocities of Tse and co-workers were reduced by 4, 5, 6, 12, 15 and 16% respectively at $\phi = 1.5$ to those predicted by the Mueller *et al.* mechanism.

2. The reduction in H_2/O_2/He burning velocities was enhanced at high pressures (10–

20 atm) by the increase in the third body efficiency of water from 12 to 14 for the reaction $\dot{H} + O_2 + M = H\dot{O}_2 + M$ but offset by the third-body efficiency of H_2 for the reaction $\dot{H} + \dot{O}H + M = H_2O + M$ which is recommended in GRI-Mech 3.0 [61]. Measurements of the rate of the reaction $\dot{H} + O_2 + M = H\dot{O}_2 + M$ where $M = H_2O$ at temperatures greater than 900 K exhibit a wide variation. We use the rate expression of $3.5 \times 10^{16} T^{-0.41} \exp(+564/T)$ cm^6 mol^{-2} s^{-1} as recommended by Mueller *et al.* Shock tube and flame studies have reported third-body efficiencies for H_2O compared to argon from 4 to 44 [80]. In their study of this reaction Hanson *et al.* [80] determined that their data, at 1,100 K and 35 atm, indicated a third-body efficiency of 17.8 for water relative to argon, consistent with the value used in GRI-Mech v2.11 [81]. This result is also in agreement with the work of Ashman and Haynes [82] in the temperature range 750–900 K and at atmospheric pressure. For the reaction $\dot{H} + O_2 + M = H\dot{O}_2 + M$ we use an efficiency of 0.67 for Ar and do not include a separate rate expression for this reaction when the third body is argon Oas do Mueller *et al.* Our efficiency of 14 for H_2O is equivalent to a H_2O:Ar effective ratio of 21:1. The Bromly *et al.* [83] rate constant of $k_0 = 2.6 \times 10^{15} \exp(+679.4/T)$ cm^6 mol^{-2} s^{-1} which was used in the Stanford study is approximately 1.4 times faster at 900 K than the value of recommended by Mueller *et al.* and used also by us. As our rate expression is lower than that recommended by Hanson *et al.*, an increase in the efficiency of water will increase our rate of reaction, consistent with the Hanson study.

3. The reduction in the enhanced third body efficiency of H_2 from 2.5 to 1.3 for the reaction $\dot{H} + O_2 + M = H\dot{O}_2 + M$ counter-acted the lowering of high-pressure burning velocities by 6% as did the new third body efficiency of H_2 for the reaction $\dot{H} + \dot{O}H + M = H_2O + M$, but only by 1%. In a recent study, Michael *et al.* quoted three values from previous work [84–86] for the H_2 collision efficiency of 1.37, 1.1 and 1.4 respectively (relative to N_2), thus our choice of 1.3 here seems entirely justified.

Burner Stabilised Flame

In an elegant series of experiments Vandooren *et al.* [35] measured species concentrations as a function of the distance above the burner in a premixed, flat flame at an equivalence ratio of 1.91 and at an initial pressure of 35.5 torr.

The experimental flame temperature profile was used in modeling the data and the same re-gridding strategy was used as in the freely propagating flame, described above. Both the original and the revised mechanisms predict essentially the same species profiles and are in reasonable agreement with experiment, Fig. 21.

There is some discrepancy between the models and experimental oxygen profile in the preheating zone of the flame front close to the burner. The maximum experimental and computed concentrations of water are identical as are the gradients of water formation. Shifting the experimental profile for water only 1.5 mm towards the burner surface would result in much better agreement.

These H_2 burner-stabilised flames can only be properly simulated if radical quenching on the burner surface is factored into the computation. The double peak in the computed OH profile, Fig. 22, is an artefact caused by neglect of radical quenching on the burner surface. This was not done in *this study* because this data was not used to validate any changes to the mechanism.

Fig. 22 shows the comparison of the $\dot{H}$, $\dot{O}$ and $\dot{O}H$ concentration profiles [35] with those predicted by our mechanism and that of Mueller *et al.* For the radicals, the model predictions are higher than the measured values. The computed profile for the intermediate species shows the same profile behaviour as the experimental one but the concentrations are overestimated by up to a factor of two for $\dot{H}$ and $O\dot{H}$ radicals in the flame and post-flame zones and by a factor of five for the $\dot{H}$ atom in the same region. Both model profiles are in close agreement with each other.

The experimental flame structure is a demanding test of the kinetic mechanism because the detection method of laser induced fluorescence, used by these workers [35], is both non

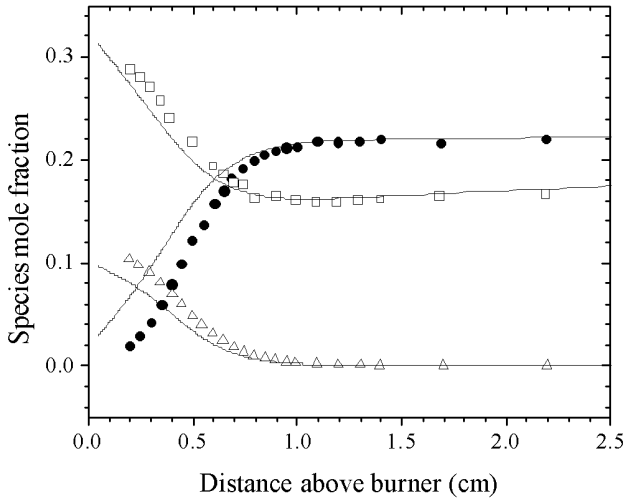

Figure 21: Species profiles in a 39.7% H_2 + 10.3% O_2, balance Ar, low-pressure burner stabilised flame from Vandooren *et al.* [35]: □ H_2, △ O_2, • H_2O; —— *this study* and Mueller *et al.*

intrusive and sensitive.

Dixon-Lewis *et al.* [33] measured species concentrations over a flat, premixed, fuel rich $H_2/O_2/N_2$ flame. The experimental temperature profile was used in simulations and good agreement found for O_2 and H_2O profiles, although that for hydrogen is much poorer. Overall for the same species, we find much better agreement of our model with the more recent measurements of Vandooren *et al.* [35].

Flow Reactor

Experiments carried out in an adiabatic flow reactor provide a well-characterised environment that is designed to minimize mixing and diffusion effects [87, 88]. Simulations were performed under the assumptions of plug flow:

- the velocity and temperature profiles in the reactor are radially uniform
- axial diffusion of both species and energy is negligible
- constant pressure and adiabatic walls were also assumed

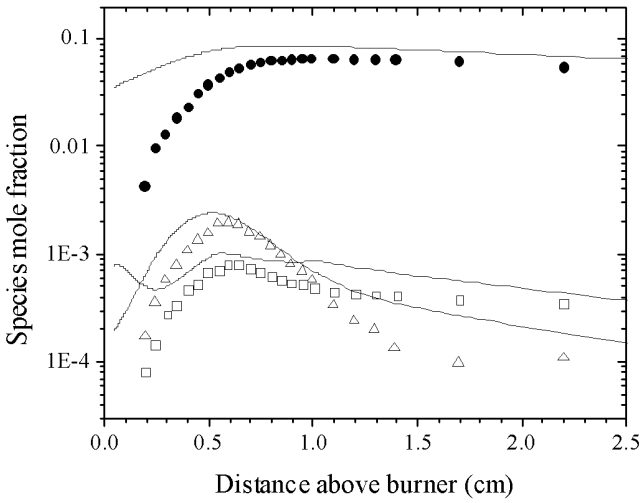

Figure 22: Species profiles in a 39.7% $H_2 + 10.3\%$ O_2, balance Ar, low-pressure burner stabilised flame from Vandooren *et al.* [35]: • $\dot{H}$, △ $\dot{O}$, □ $\dot{O}H$; —— *this study* and Mueller *et al.*

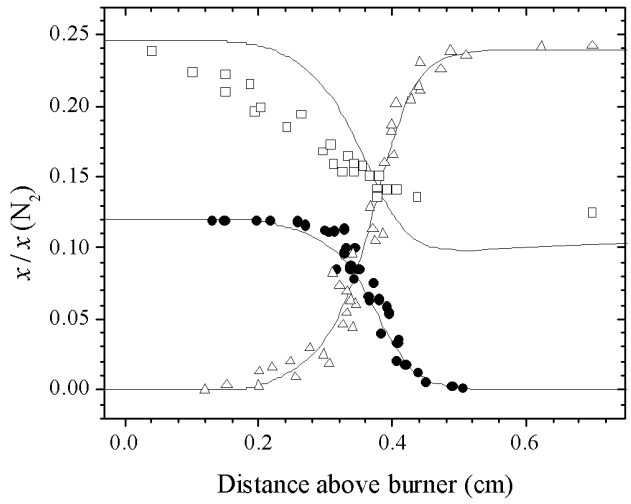

Figure 23: Species profiles in atmospheric pressure 18.83% $H_2 + 4.6\%$ O_2, balance N_2, burner stabilised flame from Dixon-Lewis *et al.* [33]: □ H_2, • $O_2/2$, △ $H_2O/2$; —— *this study* and Mueller *et al.*

Figure	P	T_i	% H_2	% O_2	Time shifts (s)	
	(atm)	(K)			*this study*	Mueller mech.
24 [6]	0.60	897	0.50	0.34	−0.068	−0.068
	0.60	896	0.50	0.76	−0.039	−0.039
25 [6]	0.30	880	0.50	0.50	−0.066	−0.066
26 [6]	2.55	935	1.01	0.52	−0.248	−0.290
	3.02	934	0.95	0.49	−0.114	−0.160
	3.44	933	1.01	0.52	−0.250	−0.290
	6.00	934	1.01	0.52	−0.360	−0.400
27 [6]	2.55	935	1.01	0.52	−0.250	−0.290
	2.50	943	1.01	1.50	−0.180	−0.205
28 [6]	15.7	914	1.18	0.61	−0.360	−0.450
	15.7	914	1.18	2.21	−0.365	−0.440
29 [6]	6.50	884	1.29	2.19	−0.320	−0.450
	6.50	889	1.30	2.21	−0.600	−0.720
	6.50	906	1.32	2.19	−0.480	−0.550
	6.50	914	1.36	2.24	−0.400	−0.460
	6.50	934	1.36	2.24	−0.250	−0.250
30 [36]	1.00	910	0.842	1.052	−0.229	−0.228

Table 4: Initial conditions for the flow reactor data of Mueller *et al.* [6] and Yetter and co-workers [36], along with model profile timeshifts. Nitrogen makes up the balance.

Mueller and co-workers [6] measured H_2, O_2, N_2 reaction profiles in a flow reactor at temperatures from 880 to 935 K and at pressures from 0.30 to 15.7 atmospheres for a number of moderately lean to moderately rich mixtures. In simulating these flow reactor results, the technique of 'time shifting' was used [89]; this makes allowance for non-ideal mixing at the reactor inlet. In essence, the calculated values are shifted along the time axis until the value for 50% fuel consumption exactly matches the experimental value. Time shifts used in carrying out the simulations are shown in Table 4.

Figs. 26–29 compare simulations to the experimental data. Both mechanisms are in excellent agreement with the experimental data as well as each other; at all conditions both mechanisms exhibit identical behaviour, Figs. 25–30.

The variation of hydrogen mole fraction with residence time at 934±1 K for four mixtures, all of the following composition: $1 \pm 0.05\%$ H_2, $0.5 \pm 0.02\%$ O_2, balance N_2 is illustrated in Fig. 26 at pressures of 2.55, 3.02, 3.44 and 6.0 atm. Both models predict

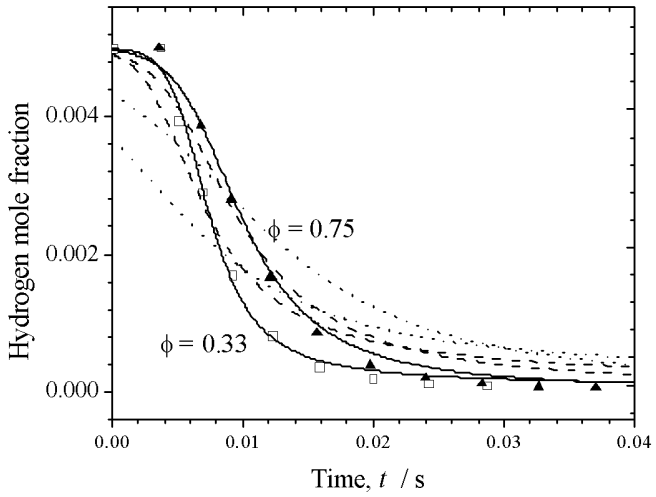

Figure 24: Flow reactor hydrogen mole fraction [6] *versus* residence time for 0.5% H_2, at 896 K and 0.6 atm: □ $\phi = 0.33$, ▲ $\phi = 0.75$; —— *this study* and Mueller *et al.*, - - - Leeds 1.5, ··· GRI-Mech 3.0 and Konnov 0.5.

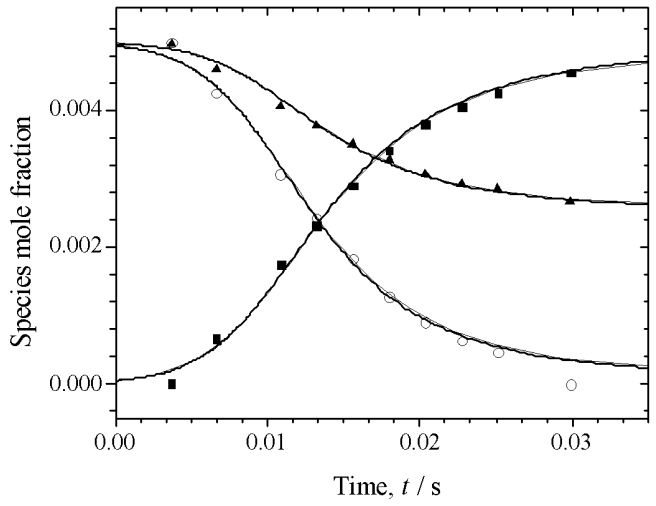

Figure 25: Flow reactor species [6] *versus* residence time for 0.5% H_2 + 0.5% O_2 in N_2, at 880 K and 0.3 atm; ○ H_2, ▲ O_2, ■ H_2O; —— *this study* Chemkin 3.6.2, 3.7 and HCT and Mueller *et al.*

essentially the same rate of hydrogen consumption and are in good agreement with experiment except for the 6.0 atm data which is initially faster than the experiments. Fig 25 illustrates the perfomance of the latest and previous Chemkin codes along with the HCT code. There is no difference in the simulation with either of these codes.

The reaction $\dot{H} + O_2 + M = H\dot{O}_2 + M$ exhibits large sensitivity at around 3 atm in this set of flow reactor data and simulations were very sensitive to modifications to most of the kinetic parameters of this reaction.

Fig. 27 illustrates an example where the mechanisms do not perform as well at lean hydrogen conditions and 2.5 atm. The stoichiometric fuel simulated profile at the same pressure performs a lot better.

For the highest pressure experiments at 15.7 atm the two mechanisms are in excellent agreement with each other and with experiment, Fig. 28.

Both the *this study* and the Princeton mechanism are in very good agreement with each other and with the experiments of Yetter *et al.* [36] who measured hydrogen, oxygen and water mole fractions as a function of residence time at 1 atm and 910 K for a 0.842% H_2, 1.052% O_2, 98.106% N_2 mixture. The concentrations of water are slightly overestimated for times of less than twelve milliseconds and slightly underestimated for times greater than eighteen milliseconds, Fig. 30.

Sensitivity Analysis

Having carried out a detailed sensitivity analysis of each of the nineteen H_2/O_2 reactions for the shock tube, flow reactor and free flame, the sensitive reactions were identified as:

$$\begin{aligned} \dot{H} + O_2 &= O + \dot{O}H \\ \dot{O} + H_2 &= \dot{H} + \dot{O}H \\ \dot{O}H + H_2 &= \dot{H} + H_2O \\ \dot{O} + H_2O &= \dot{O}H + \dot{O}H \end{aligned}$$

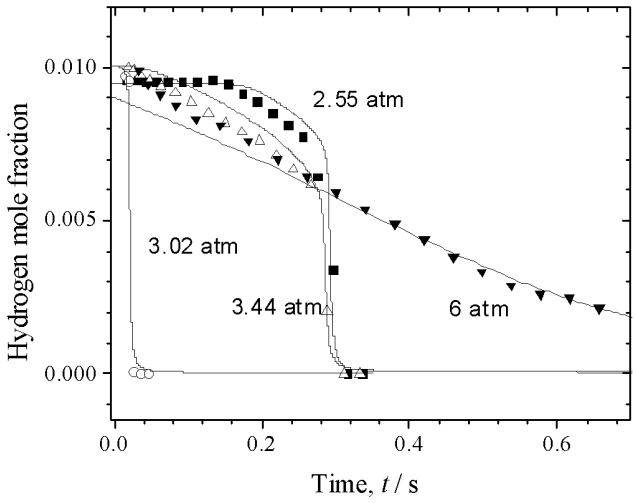

Figure 26: Flow reactor [6] hydrogen mole fraction *versus* residence time at 934 ± 1 K for a 1.01% H_2 + 0.52% O_2, balance N_2, mixture *except* 3.02 atm which is 0.95% H_2 + 0.49% O_2. ■ 2.55 atm, ○3.02 atm, △ 3.44 atm, ▼ 6.00 atm; —— *this study* and Mueller *et al.*

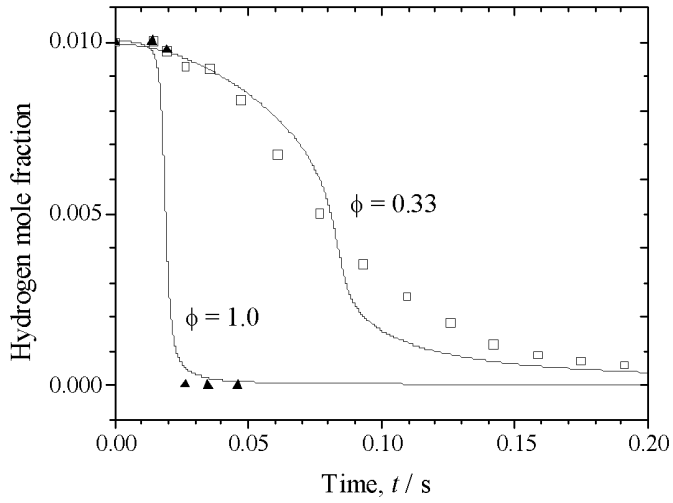

Figure 27: Flow reactor [6] hydrogen mole fraction *versus* residence time, at 2.5±0.05 atm, ▲ 935 K, 0.5% H_2 + 0.52% O_2 in N_2; □ 943 K, 1.01% H_2 + 1.5% O_2 in N_2; —— *this study* and Mueller *et al.*

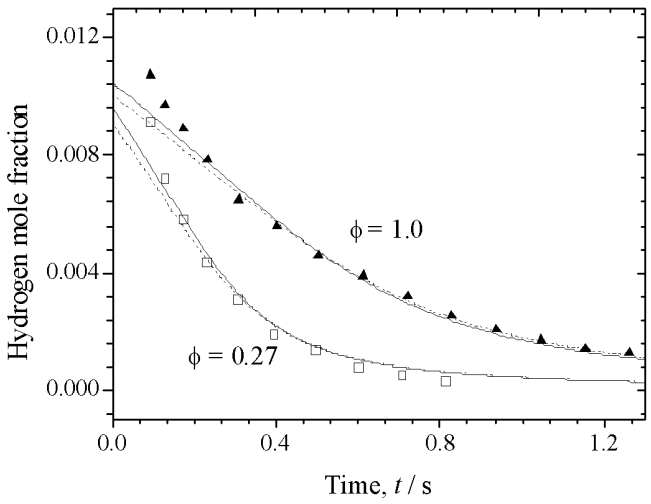

Figure 28: Flow reactor [6] hydrogen mole fraction *versus* residence time, at 15.71 atm and 914 K: ▲ 1.18% H_2 + 2.21% O_2 in N_2, □ 1.18% H_2 + 0.61% O_2 in N_2; —— *this study*, – – – Mueller *et al.*

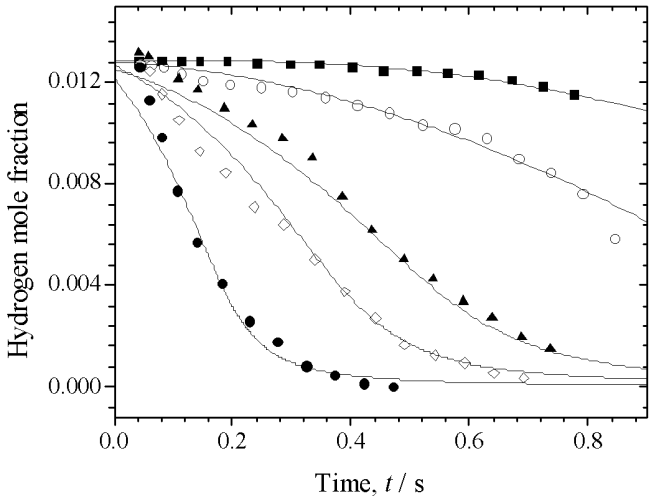

Figure 29: Flow reactor [6] hydrogen mole fraction *versus* residence time [6], at 6.5 atm, 1.3% H_2, 2.2% O_2: ■ 884 K, ○ 889 K, ▲ 906 K, ◇ 914 K, ● 934 K; —— *this study* and Mueller *et al.*

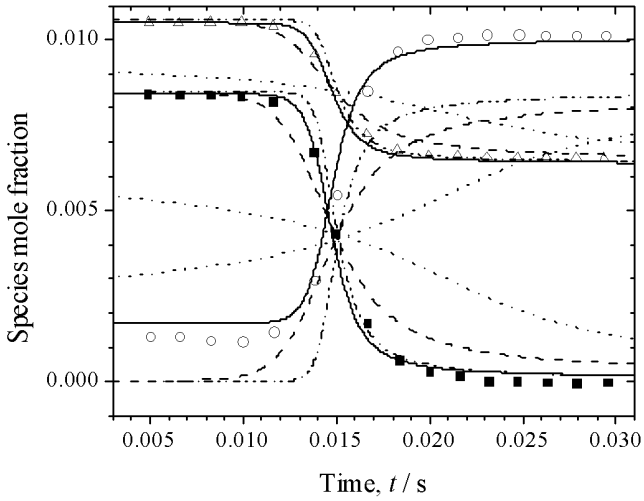

Figure 30: Flow reactor [36] hydrogen mole fraction *versus* residence time at 1.0 atm and 910 K: ■ H_2, △ O_2, ○ H_2O; model predictions: —— *this study* and Mueller *et al.*, - - - Leeds 0.5, · · · GRI-Mech 3.0, — · · Konnov 0.5.

$$\begin{aligned}
\dot{\mathrm{H}} + \dot{\mathrm{O}}\mathrm{H} + \mathrm{M} &= \mathrm{H_2O} + \mathrm{M} \\
\dot{\mathrm{H}} + \mathrm{O_2} + \mathrm{M} &= \mathrm{H}\dot{\mathrm{O}}_2 + \mathrm{M} \\
\mathrm{H}\dot{\mathrm{O}}_2 + \dot{\mathrm{H}} &= \mathrm{H_2} + \mathrm{O_2} \\
\mathrm{H}\dot{\mathrm{O}}_2 + \dot{\mathrm{H}} &= \dot{\mathrm{O}}\mathrm{H} + \dot{\mathrm{O}}\mathrm{H} \\
\mathrm{H_2O_2} + \dot{\mathrm{H}} &= \mathrm{H_2} + \mathrm{H}\dot{\mathrm{O}}_2
\end{aligned}$$

These reactions were investigated further to determine whether modifying their rate constants resulted in an overall improvement in the models' agreement with the experimental data sets. Sensitivity analyses were carried out on five of the H_2/O_2 datasets which encompass the four combustion environments studied: Slack's ignition delay calculations, the atmospheric flame speed measurements of Dowdy *et al.*, the H_2/O_2/He mass burning velocities of Tse *et al.* and the species concentration profiles of Mueller *et al.* The reaction $\dot{\mathrm{H}} + \mathrm{O_2} = \mathrm{O} + \dot{\mathrm{O}}\mathrm{H}$ was not investigated; there are several more recent studies that have reported rate constants for this reaction. Those used in the major reaction mechanisms

are Pirraglia *et al.* [39] (*this study*), Yu *et al.* [90], Baulch *et al.* [46] Ryu *et al.* [91] and Hessler [92]. In his study, Hessler notes a 94.5% confidence envelope in the data. Troe [93] has very recently published a comprehensive review of this reaction from the earliest studies of Ostwald to the latest recommended value, $3.43 \times 10^{-10} T^{-0.097} \exp(-7560/T)$ cm^6 molecule^{-2} s^{-1} [94].

Altering the channel ratio for the reactions:

$$\begin{aligned} \mathrm{H\dot{O}_2 + \dot{H}} &= \mathrm{H_2 + O_2} \\ \mathrm{H\dot{O}_2 + \dot{H}} &= \mathrm{\dot{O}H + \dot{O}H} \end{aligned}$$

in any way was found to have an adverse effect on the flow reactor simulations. Therefore we neither altered the channel ratio nor the total rate. Where appropriate, rate constants were only changed within the bounds of previously reported experimental and review data contained in the NIST database [79].

Sensitivity analyses were performed by multiplying the rate constant of each individual reaction by two and calculating the change in the appropriate parameter.

Ignition Delay Times in a Shock Tube

In the case of shock tube sensitivity calculations, Fig. 31, a baseline ignition delay time was computed for a given set of physical conditions used in Fig. 8. The rate constant of each reaction was individually multiplied by two and the new 'perturbed' ignition delay time calculated for the kinetic mechanism perturbed by the reaction in question. The percent change in the ignition delay time was recorded as the 'percent sensitivity' of that particular reaction. A positive value indicates a longer ignition delay and conversely a negative value points to a shorter ignition delay time. The reaction with the highest negative sensitivity is therefore the most effective in promoting the overall rate of oxidation.

The sensitivity analysis, Fig. 31, indicates that the ignition delay time is very sensitive to the reaction $\mathrm{\dot{H} + O_2 + M = H\dot{O}_2 + M}$, with the reactions:

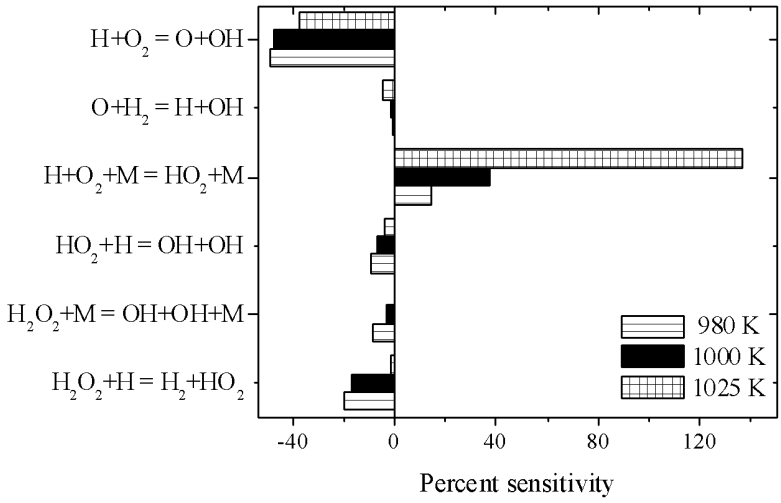

Figure 31: Sensitivity analysis of shock tube experiments [15]. Sensitivity of $\dot{\mathrm{H}} + \mathrm{O}_2 + \mathrm{M} = \mathrm{H}\dot{\mathrm{O}}_2 + \mathrm{M}$ is plotted to 1/10 scale.

$$\begin{aligned} \dot{\mathrm{H}} + \mathrm{O}_2 &= \dot{\mathrm{O}} + \dot{\mathrm{O}}\mathrm{H} \\ \mathrm{H}_2\mathrm{O}_2 + \dot{\mathrm{H}} &= \mathrm{H}_2 + \mathrm{H}\dot{\mathrm{O}}_2 \end{aligned}$$

also showing appreciable sensitivity.

The model ignition delay times are significantly slower than the experiments, Fig. 8, especially at lower temperatures. To compensate for this, the enhanced third body coefficient of H_2 for the reaction $\dot{\mathrm{H}} + \mathrm{O}_2 + \mathrm{M} = \mathrm{H}\dot{\mathrm{O}}_2 + \mathrm{M}$ was reduced from 2.5 to 1.3. The simulated ignition delay times of Slack, Fig. 8, are three times faster than Mueller *et al.* at 980 K and the revised mechanism is in excellent agreement with experiments. The revised simulated experimental profile of Fujimoto is also an improvement to the agreement with the photometric ignition delay measurements below 1020 K.

An interesting result of the shock tube sensitivity analysis is that the reaction $\mathrm{H}_2\mathrm{O}_2 + \dot{\mathrm{H}} = \mathrm{H}_2 + \mathrm{H}\dot{\mathrm{O}}_2$ is a significant feature of this combustion environment only. There

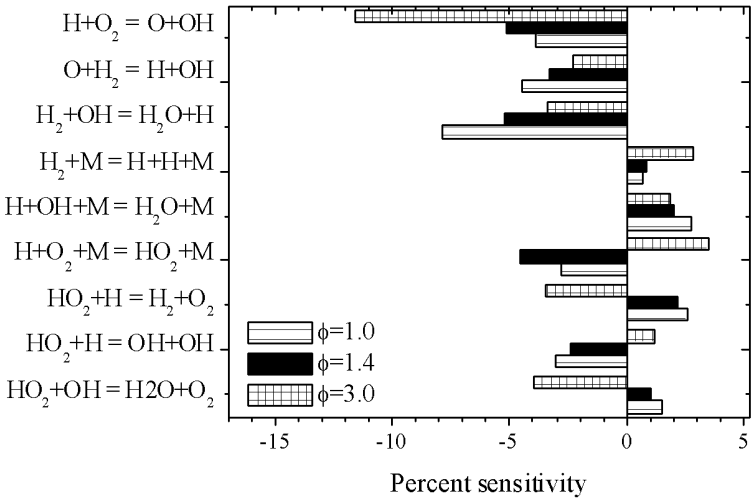

Figure 32: Flame speed sensitivity analysis of a freely propagating H_2, O_2 in air flame [29] at 1 atm.

are very few measurements of the rate for this reaction at the relevant temperatures, Fig. 3.

Freely Propagating Flames

A sensitivity analysis of the mechanism was carried out on flame speed/mass burning rate calculations at equivalence ratios of 1.0, 1.4 and 3.0 [29], Fig. 32, and, 1.0, 1.5 and 2.5 [31], Fig. 33. The baseline or unperturbed flame speed was computed for a given set of physical conditions used in Fig. 16 and Fig. 17. The rate constant of each reaction was individually multiplied by two and the new 'perturbed' flame speed calculated for the kinetic mechanism perturbed by the reaction in question. The percent change in the flame speed was recorded as the 'percent sensitivity' of that particular reaction.

Perturbing the A factor by a factor of two in this case does not result in any large sensitivities. However, it is pertinent to discuss relative sensitivities so that we can see which reactions are dominating the combustion environment. The largest sensitivity of -12% is due to: $\dot{\mathrm{H}} + \mathrm{O}_2 = \dot{\mathrm{O}} + \dot{\mathrm{O}}\mathrm{H}$. Significantly, the reaction $\dot{\mathrm{H}} + \dot{\mathrm{O}}\mathrm{H} + \mathrm{M} = \mathrm{H}_2\mathrm{O} + \mathrm{M}$ shows slight positive sensitivity here but was very insensitive to the ignition delay measure-

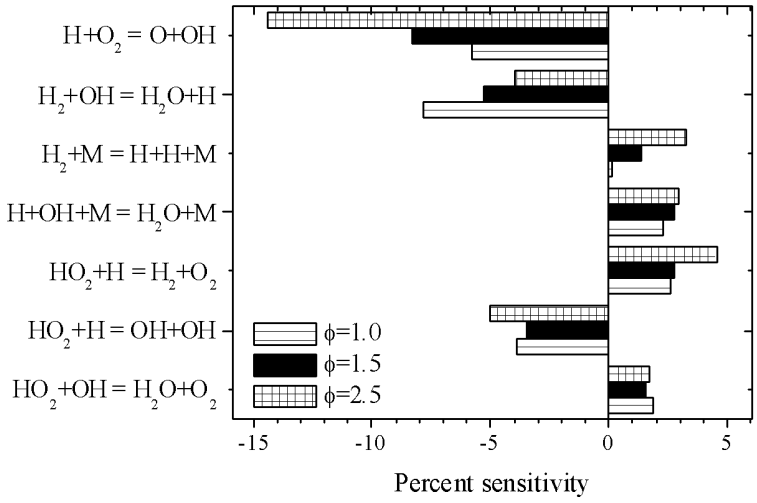

Figure 33: Flame speed sensitivity analysis in a freely propagating flame [31] at 5 atm.

ments, Fig. 31, and to the flow reactor experiments, Fig. 34. This allowed us to increase the previously recommended reaction rate by a factor of two which reduced the computed maximum flame speed by 6% at an equivalence ratio of 1.7 but which had no effect on the computed ignition delay times or the calculated flow reactor concentrations. However, this increase was slightly offset by the increase in the enhanced third body efficiency of H_2O for the reaction $\dot{H} + O_2 = \dot{O} + \dot{O}H$.

The Tse *et al.* flame speeds show similar sensitivities, Fig. 33, with the notable exception of the $\dot{H} + O_2 + M = H\dot{O}_2 + M$ reaction which does not feature at stoichiometric and rich conditions up to 5 atm. The reaction $\dot{H} + \dot{O}H + M = H_2O + M$ is not sensitive at 5 atm, but the increase in its rate is primarily responsible for the progressively slower maximum mass burning velocities with increasing pressure, described in the Kinetic modeling section. The reaction $\dot{H} + O_2 + M = H\dot{O}_2 + M$ does not feature in the sensitivity analysis carried out at five atm. We found, however, that between ten and twenty atm, this reaction is primarily responsible for the reduction in mass burning rates, Fig. 18. The mass burning velocities are an excellent fit to the experimental measurements especially at increasing pressures.

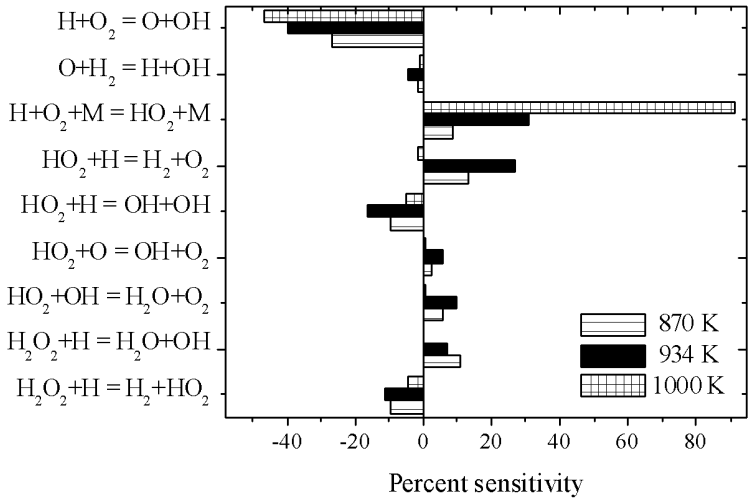

Figure 34: Flow reactor sensitivity analysis at 20% fuel conversion, 3.02 atm, 934 K, 0.95% H_2, 0.49% O_2 and 98.56% N_2 [6]. Sensitivity to the reaction $\dot{H} + O_2 + M = H\dot{O}_2 + M$ is plotted to 1/2 scale.

Variable Pressure Flow Reactor

The flow reactor percent sensitivities were evaluated as the percent difference between the 'baseline' calculation for the consumption of 20% hydrogen and the 'perturbed' calculation for the consumption of 20% hydrogen at 870 K, 934 K and 1,000 K, 3.02 atm, 0.95% H_2 + 0.49% O_2 and balance N_2. The flow reactor was not sensitive to the alteration of the rate of the reaction $\dot{H} + \dot{O}H + M = H_2O + M$ and only very slightly sensitive to that for $H_2O_2 + \dot{H} = H_2 + H\dot{O}_2$.

COMPARISONS

Davis *et al.* [8] recently published a CO-H_2-O_2 modeling study using many of the latest reported rate constants for reactions such as $H\dot{O}_2 + \dot{H} = H_2 + O_2$ and $\dot{H} + O_2 + M = H\dot{O}_2 + M$. Interestingly, the authors used a pressure-dependent rate constant for the reaction $\dot{H} + \dot{O}H + M = H_2O + M$. We found that using a similar expression adversely affected the performance of our mechanism in all cases. The differences in the performance of the two mechanisms are as

follows:

1. Their simulations for the shock tube experiments of Slack [15] are considerably worse than ours and lie closer to those of Mueller *et al.* [6], Fig. 8.

2. Their predicted laminar flame speeds for H_2/O_2/He mixtures at elevated pressures are much faster than those reported by Tse *et al.*, with which we are in good agreement.

We have also compared the performance of our mechanism with the H_2+O_2 submechanisms of a number of recent methane oxidation schemes, namely Konnov [59, 60], Leeds [58] and GRI-Mech [61]. We found that none of these reproduce the experiments with the consistency of *this study*. Although the agreement with experiments can be dramatically worse or somewhat better than the *revised mechanism*, the hydrogen mechanism presented here has been proven to perform much more consistently over a wider range of experimental conditions.

The mechanism of this study reproduces all shock tube data with greater success than the others. The *revised mechanism* is the only one that can be said to satisfactorily reproduce all of the flame speed experiments, Figs. 16–20. It must be noted, however, that the Leeds, Konnov and GRI-Mech mechanisms do not contain helium; in order to compute flame speeds with these particular mechanisms we employed the argon parameters to simulate the helium-containing mixtures.

The atmospheric flame data, Fig. 16, is well reproduced by all the mechanisms, with Mueller *et al.* and GRI-Mech being the fastest and slowest respectively at $\phi \geq 2.0$. Below $\phi = 2$, Konnov and Leeds are slowest and Mueller *et al.* is fastest.

Although it has been argued recently [95] that the modeling uncertainties in flow reactor data are very large, *this study* and Mueller *et al.* are the only two available mechanisms that reproduce the data satisfactorily, Fig. 24.

Mueller *et al.* [6] have noted that chain branched reactions, which dominate at low pressures, are well understood but for a comprehensive oxidation mechanism to be suc-

cessful at simulating experiments over a wide range of conditions, the reactions of H_2O_2 and $H\dot{O}_2$ must be taken into account; that is the case for all the mechanisms considered here.

All four mechanisms have the same number of species and reactions, differing only in small details. However these details are important because they do give rise to different predictions as illustrated above. However the converse may also apply with substantial differences in a particular rate expression resulting in essentially the same predictions. For example, for the two sensitive reactions below, GRI-Mech and Konnov use quite diffent rate constants, yet the results are quite similar:

Reaction	[60]	[61]
$\dot{H} + O_2 + M = H\dot{O}_2 + M$	$1.48 \times 10^{12}\ T^{0.6}$	$2.8 \times 10^{18}\ T^{-0.86}$
$\dot{H} + O_2 = \dot{O} + \dot{O}H$	$9.75 \times 10^{13} e^{(+7.75/T)}$	$2.65 \times 10^{16}\ T^{-0.67} e^{(+8.58/T)}$

CONCLUSIONS

The present study has refined an existing hydrogen reaction mechanism using the best available kinetic data and sound thermochemical analyses. The mechanism has been rigorously tested by comparing computed results with a wide range of data reported by a number of authors using a variety of experimental techniques. Agreement between computed and measured results was good and suggests strongly that the great majority of the reported reaction paths and rate expressions are reasonably correct. We are confident that the changes made to the mechanism have improved the performance, as against existing models, over a wider range of physical conditions. It is expected that this study will act as a basis for the modeling of larger hydrocarbons under a wide range of physical conditions.

Acknowledgements

We thank the Higher Education Authority of Ireland for financial support (PRTLI-II) and Enterprise Ireland for an International Collaboration award.

BIBLIOGRAPHY

[1] Heffel, J. W.; Int J Hydrogen Energy 2003, 28, 1285–1292.

[2] Schlapbach, L.; Zuttel, A.; Nature 2001, 414, 353–358.

[3] Hirscher, M.; Becher, M.; J Nanosci Nanotech 2003, 3, 3–17.

[4] Simmie, J.M.; Prog Energy Combust Sci 2003, 29, 599–643.

[5] Smith, G.P.; *Diagnostics for Detailed Kinetic Modeling* in *Applied Combustion Diagnostics*, Kohse-Höinghaus, K.; Jeffries, J.B.; ed. Taylor and Francis, N.Y. (2002).

[6] Mueller, M.A.; Yetter, R.A.; Dryer, F.L.; Int J Chem Kinet 1999, 31, 113–125.

[7] Marinov, N. M.; Westbrook, C. K.; Pitz, W. J.; Transport Phenomena in Combustion, 118–129.

[8] Davis, S.G.; Joshi, A.V.; Wang, H.; Egolfopoulos, F.N.; *Proceedings of the Third Joint Meeting of the U.S. Sections of the Combustion Institute* Chicago, Illinois, USA. Work in Progress Paper A08 (2003).

[9] Schott, G.L.; Kinsey, J.L.; J Chem Phys 1958, 29, 1177–1182.

[10] Skinner, G.B.; Ringrose, G.H.; J Chem Phys 1965, 42, 2190–2192.

[11] Asaba, T.; Gardiner, W.C.; Stubbeman, R.F.; Proc Combust Inst 1965, 10, 295–302.

[12] Fujimoto, S.; Suzuki, M.; Memoirs Defense Academy, Japan, Vol. VII 1967, 3, 1037–1046.

[13] Hasegawa, K.; Asaba, T.; J Faculty of Engineering, The University of Tokyo (B) 1972, 31, 515.

[14] Bhaskaran, K.A.; Gupta, M.C.; Just, Th.; Comb Flame 1973, 21, 45–48.

[15] Slack, M.W.; Comb Flame 1977, 28, 241–249.

[16] Cheng, R.K.; Oppenheim, A.K.; Comb Flame 1984, 58, 125–139.

[17] Koike, T.; Bull Chem Soc Japan 1989, 62, 2480–2484.

[18] Hidaka, Y.; Sato, K.; Henmi, Y.; Tanaka, H.; Inami, K.; Comb Flame 1999, 118, 340–358.

[19] Petersen, E.L.; Davidson, D.F.; Röhrig, M.; Hanson, R.K.; 20th Int Symp Shock Waves 1996, 941–946.

[20] Petersen, E.L.; Kalitan, D.M.; Rickard, M.J.A.; *Proceedings of the Third Joint Meeting of the U.S. Sections of the Combustion Institute* Chicago, Illinois, USA. Papers C25/PL05 (2003).

[21] Wang, B.L.; Olivier, H.; Grönig, H.; Comb Flame 2003, 133, 93–106.

[22] Koroll, G.W.; Kumar, R.K.; Bowles, E.M.; Comb Flame 1993, 94, 330–40.

[23] Iijima, T.; Takeno, T.; Comb Flame 1986, 65, 35–43.

[24] Takahashi, F.; Mizomoto, M.; Ikai, S.; Alternative Energy Sources III 1983, 5, 447–457.

[25] Wu, C.K.; Law, C.K.; Proc Combust Inst 1984, 20, 1941–1949.

[26] Egolfopoulos, F.N.; Law, C.K.; Proc Combust Inst 1990, 23, 333–340.

[27] Law, C.K.; in *Reduced Kinetic Mechanisms for Applications in Combustion Systems*, (N. Peters and B. Rogg, eds.) Springer–Verlag, Berlin. (1993).

[28] Vagelopoulos, C.M.; Egolfopoulos, F.N.; Law, C.K.; Proc Combust Inst 1995, 25, 1341–1347.

[29] Dowdy, D.R.; Smith, D.B.; Taylor, S.C.; Proc Combust Inst 1990, 23, 325–332.

[30] Aung, K.T.; Hassan, M.I.; Faeth, G.M.; Comb Flame 1997, 109, 1–24.

[31] Tse, S.D.; Zhu, D.L.; Law, C.K.; Proc Combust Inst 2000, 28, 1793–1800.

[32] Lamoureux, N.; Djbaïli-Chaumeix, N; Paillard, C.E.; Exp Therm Fluid Sci 2003, 28, 385–393.

[33] Dixon-Lewis, G.; Sutton, M.M.; Proc Roy Soc Lond A 1970, 317, 227–234.

[34] Kohse Höinghaus, K; Kelm, S.; Meier, U.; Bittner, J.; Just, Th; Springer. Ser. Chem. Phys. (Complex Chem React Sys) 1987, 47, 292–301.

[35] Vandooren, J.; Bian, J.; Proc Combust Inst 1990, 23, 341–346.

[36] Yetter, R.A.; Dryer, F.L.; Rabbitz, H.; Combust Sci Technol 1991, 79, 129–140.

[37] Lund, C. M., *HCT – A General Computer Program for Calculating Time-Dependent Phenomena Involving One-Dimensional Hydrodynamics, Transport, and Detailed Chemical Kinetics*, Lawrence Livermore National Laboratory report revised (1995).

[38] Kee, R.J.; Rupley, Miller, J.A.; Coltrin, M.E.; F.M.; Grcar, J.F.; Meeks, E.; Moffat, H.K.; Lutz, A.E.; Dixon-Lewis, G.; Smooke, M.D.; Warnatz, J.; Evans, G.H.; Larson, R.S.; Mitchell, R.E.; Petzold, L.R.; Reynolds, W.C.; Caractsios, M.; Stewart, W.E.; Glarborg, P.; Wang, C.; Adigun, O.;*Chemkin Collection*, Release 3.6, Reaction Design, Inc., San Diego, CA, 2000.

[39] Pirraglia, A.N.; Michael, J.V.; Sutherland, J.W.; Klemm, R.B.; J Phys Chem 1989, 93, 282–291.

[40] Sutherland, J.W.; Michael, J.V.; Pirraglia, A.N.; Nesbitt, F.L.; Klemm, R.B.; Proc Combust Inst 1986, 21, 929–941.

[41] Michael, J.V.; Sutherland, J.W.; J Phys Chem 1988, 92, 2853–3857.

[42] Sutherland, J.W.; Patterson, P.M.; Klemm, R.B.; Proc Combust Inst 1990 23, 51–57.

[43] Tsang, W.; Hampson, R.F.; J Phys Chem Ref Data 1986, 15, 1087–1279.

[44] Mueller, M.A.; Yetter, R.A.; Dryer, F.L.; Proc Combust Inst 1998, 27, 177–184.

[45] Cobos, C.J.; Hippler, H.; Troe, J.; J Phys Chem 1985, 89, 342–349.

[46] Baulch, D.L.; Cobos, C.J.; Cox, R.A.; Frank, P.; Hayman, G.; Just, Th.; Kerr, J.A.; Murrells, T.; Pilling, M.J.; Troe, J.; Walker, R.W.; Warnatz, J.; J Phys Chem Ref Data 1994, 23, 847–1033.

[47] Hippler, H.; Troe, J.; Willner, J.; J Chem Phys 1993, 90, 1755–1760.

[48] Warnatz, J.; in Combustion Chemistry, Gardiner, W. C., Ed., Springer-Verlag: New York, NY, 1985.

[49] Brouwer, L.; Cobos, C.J.; Troe, J.; Dubal, H.R.; Crim, F.F.; J Chem Phys 1985, 86, 6171–6182.

[50] Hippler, H.; Troe, J.; Chem Phys Lett 1992 4, 333–337.

[51] Kee, R.J.; Rupley, F.M.; Miller, J.A.; Sandia National Laboratories Report SAND87–8217, 1987.

[52] Hills, A.J.; Howard, C.J.; J Chem Phys 1984 81, 4458–4465.

[53] Ramond, T.M.; Blanksby, S.J.; Kato, S.; Bierbaum, V.M.; Davico, G.E.; Schwartz, R.L.; Lineberger, W.C.; Ellison, G.B.; J Phys Chem A 2002, 106, 9641–9647.

[54] Ruscic, B.; Wagner, A.F.; Harding, L.B.; Asher, R.L.; Feller, D.; Dixon, D.A.; Peterson, K.A.; Song, Y.; Qian, X.M.; Ng, C.Y.; Liu, J.B.; Chen, W.W.; J Phys Chem A 2002, 106, 2727-2747.

[55] Herbon, J.T.; Hanson, R.K.; Golden, D.M.; Bowman, C.T.; Proc Combust Inst 2003, 29, 1201–1208.

[56] Yetter, R.A.; Dryer, F.L.; Rabbitz, H.; Combust Sci Technol 1991, 79, 97–128.

[57] Kim, T.J., Yetter, R.A.; Dryer, F.L.; Proc Combust Inst 1994, 25, 759–766.

[58] Hughes, K.J.; Turäanyi, T.; Pilling, M.J.; Leeds methane oxidation mechanism. `http://www.chem.leeds.ac.uk/Combustion/methane.htm`

[59] Konnov, A.A.; *Detailed reaction mechanism for small hydrocarbons combustion; release 0.3* 1998. `http://homepages.vub.ac.be/~akonnov/`

[60] Konnov, A.A.; *Detailed reaction mechanism for small hydrocarbons combustion; release 0.5* 2000. `http://homepages.vub.ac.be/~akonnov/`

[61] Smith, G.P.; Golden, D.M.; Frenklach, M.; Moriarty, N.W.; Eiteneer, B.; Goldenberg, M.; Bowman, C.T.; Hanson, R.K.; Song, S.; Gardiner, W.C. Jr.; Lissianski, V.V.; Qin, Z.; GRI-Mech 3.0. `http://www.me.berkeley.edu/gri_mech/`

[62] Gay, A.; Pratt, N.H.; Symp Shock Tube Waves 1971, 8, 39.

[63] Baulch, D.L.; Cobos, C.J.; Cox, R.A.; Esser, C.; Frank, P.; Just, Th.; Kerr, J.A.; Pilling, M.J.; Troe, J.; Walker, R.W.; Warnatz, J.; J Phys Chem Ref Data 1992, 21, 411–429.

[64] Troe, J.; J Phys Chem 1979, 83, 114–126.

[65] Zellner, R.; Erler, K.; Field, D.; Proc Combust Inst 1977, 16, 939.

[66] Bulewicz, E.M.; Sugden, T.M.; Trans Faraday Soc 1958, 54, 1855–1860.

[67] Baldwin, R.R.; Jackson, D.; Walker, R.W.; Webster, S.J.; Trans Faraday Soc 1967, 63, 1676–1686.

[68] Lee, D.; Hochgreb, S.; Int. Int J Chem Kinet 1998, 30, 385–406.

[69] Baldwin R.F.; Walker, R.W.; J Chem Soc Faraday Trans I 1979, 75, 140–154.

[70] Gorse, R.A.; Volman, D.H.; J Photochem 1974, 3, 115.

[71] Michael, J.V.; Su, M.-C.; Sutherland, J.W.; Carroll, J.J.; Wagner, A.F.; J Phys Chem. A 2002, 106, 5297–5313.

[72] Lutz, A.E.; Kee, R.J.; Miller, J.A.; Sandia National Laboratories Report SAND87-8248, 1988.

[73] Kee, R.J.; Rupley, F.M.; Miller, J.A.; Coltrin, M.E.; Grcar, J.F.; Meeks, E.; Moffat, H.K.; Lutz, A.E.; Dixon-Lewis, G.; Smooke,; M.D. Warnatz, J.; Evans, G.H.; Larson, R.S.; Mitchell, R.E.; Petzold, L.R.; Reynolds, W.C.; Caracotsios, M.; Stewart, W.E.; Glarborg, P.; Wang, C.; Adigun, O.; Houf, W.G.; Chou, C.P.; Miller, S.F.; Chemkin Collection, Release 3.7.1, Reaction Design, Inc., San Diego, CA (2003).

[74] Mitchell, R.E.; Kee, R.J.; Sandia National Laboratories Report SAND82-8205, 1982.

[75] Kee, R.J.; Grcar, J.F.; Smooke, M.D.; Miller, J.A.; *PREMIX: A Fortran Program for Modeling Steady State Laminar One-Dimensional Flames,* Sandia Laboratories Report SAND85–8240 (1985).

[76] Breshears, W.D.; Bird, P.F.; J Phys Chem A 1968, 48, 10, 4768–4773.

[77] Hanson, R.K.; Baganoff, D.; Phys Chem A 1970, 53, 11, 4401–4403.

[78] Andrews, G.E.; Bradley, D.; Combust Flame 1972, 18, 133–153.

[79] Mallard, W.G.; Westley, F.; Herron, J.T.; Hanson, R.F.; *NIST Standard Reference Database 17 2Q98; NIST Standard Reference Data: Gaithersburg, MD. (1994).*

[80] Hanson, R.K.; Golden, D. M.; Bowman, C.T.; Davidson, D.F.; Bates, R. W.; First Joint Meeting of the U.S. Sections of the Combustion Institute, The George Washington University, Washington D.C. March 14-17, (1999).

[81] Bowman, C.T.; Hanson R.K.; Davidson, D.F.; Gardiner, W.C. Jr.; Lissianski, V.; Smith, G.P.; Golden, D.M.; Frenklach, M.; Goldenberg, M.; GRI-Mech 2.1. `http://www.me.berkeley.edu/gri_mech/`

[82] Ashman, P. J. and Haynes, B. J., Proc Combust Inst 1998, 27, 185–191.

[83] Bromly, J. H., Barnes, F. J., Nelson, P. F. and Haynes, B. S., Int J Chem Kinet 1995, 27, 1165-1178.

[84] Hidaka, T.; Eyre, J.; Dorfman, L.M.; J Chem Phys 1971, 54, 3422.

[85] Wong, W.; Davis, D.D.; Int J Chem Kinet 1974, 6, 401.

[86] Nielsen, O.J.; Sillesen, A.; Luther, K.; Troe, J.; J Phys Chem 1982, 86, 2929.

[87] Vermeersch, M.L.; Held, T.J.; Stein, Y.S., Dryer, F.L.; SAE Trans 1991, 100, 645.

[88] Callahan, C.V., Held, T.J.; Dryer, F.L.; Minetti, R.; Ribbaucour, M.; Sochet, L.R.; Faravelli, T.; Gaffuri, P.; Ranzi, E.; Proc. Combust Inst 1996, 22, 739–746.

[89] Fischer, S.L.; Dryer, F.L.; Curran, H.J.; Int J Chem Kinet 2000, 32, 713–740.

[90] Yu, C.-L.; Frenklach, M.; J Phys Chem 1994, 98, 4770–4771.

[91] Ryu, S.-O.; Hwang, S.M.; Rabinowitz, M.J.; J Phys Chem 1995, 99, 13984–13991.

[92] Hessler, J.P.; J Phys Chem A 1998, 102, 4417–4526.

[93] Troe, J.; Z Phys Chem 2003, 217, 1303–1317.

[94] Baulch, D.L.; Private communication, 2004.

[95] Zsély, I. Gy.; Zádor, J.; Turányi, T.; paper 35, Proceedings of the 3rd European Combustion Meeting, Orléans, 2003.

List of Figures